



저작자표시-비영리-변경금지 2.0 대한민국

이용자는 아래의 조건을 따르는 경우에 한하여 자유롭게

- 이 저작물을 복제, 배포, 전송, 전시, 공연 및 방송할 수 있습니다.

다음과 같은 조건을 따라야 합니다:



저작자표시. 귀하는 원저작자를 표시하여야 합니다.



비영리. 귀하는 이 저작물을 영리 목적으로 이용할 수 없습니다.



변경금지. 귀하는 이 저작물을 개작, 변형 또는 가공할 수 없습니다.

- 귀하는, 이 저작물의 재이용이나 배포의 경우, 이 저작물에 적용된 이용허락조건을 명확하게 나타내어야 합니다.
- 저작권자로부터 별도의 허가를 받으면 이러한 조건들은 적용되지 않습니다.

저작권법에 따른 이용자의 권리는 위의 내용에 의하여 영향을 받지 않습니다.

이것은 [이용허락규약\(Legal Code\)](#)을 이해하기 쉽게 요약한 것입니다.

[Disclaimer](#)

A DISSERTATION
FOR THE DEGREE OF DOCTOR OF PHILOSOPHY

DEVELOPMENT OF LARGE VOLUME AIR PLASMA
FOR PRACTICAL APPLICATION TO
GAS CONTAMINANT REMOVAL

MATYAKUBOV NOSIR SHIHNAZAROVICH

Major of Energy & Chemical Engineering
FACULTY OF APPLIED ENERGY SYSTEM
GRADUATE SCHOOL
JEJU NATIONAL UNIVERSITY

August - 2022

**DEVELOPMENT OF LARGE VOLUME AIR PLASMA FOR
PRACTICAL APPLICATION TO GAS CONTAMINANT
REMOVAL**

MATYAKUBOV NOSIR SHIHNAZAROVICH
(Supervised by Professor Young Sun Mok)

A thesis submitted in partial fulfillment of the requirement for the degree of
Doctor of Philosophy
2022. 06

The thesis has been examined and approved.

Professor Heonju Lee Thesis Director	 	Department of Energy Engineering, Jeju National University
Professor Ho Won Lee Thesis Committee Member		Department of Chemical Engineering, Jeju National University
Professor Sang Jae Kim Thesis Committee Member	 	Department of Mechanical System Engineering, Jeju National University
Professor Woo Young Kim Thesis Committee Member	 	Department of Electronic Engineering, Jeju National University
Professor Young Sun Mok Thesis Committee Member & Supervisor		Department of Chemical Engineering, Jeju National University

June - 2022

Major of Energy & Chemical Engineering
FACULTY OF APPLIED ENERGY SYSTEM
GRADUATE SCHOOL
JEJU NATIONAL UNIVERSITY

*This dissertation is dedicated to my parents,
Matyakubov Shixnazar and Ibragimova Asiljan, who have sincerely
supported and helped the upbringing and education of their four sons.*

ABSTRACT

Non-thermal plasma catalyst systems have been used for environmental control, including abatement of VOC and NO_x removal at atmospheric pressure because of their hazardous impact on the environment and human health. This dissertation investigates non-thermal corona plasma generated in a honeycomb monolith catalyst for VOC decomposition and rotational gliding arc plasma produced for NO_x reduction from the diesel exhaust gas. The general aim of the research is developing non-thermal air plasma catalyst systems to improve the removal efficiency of VOC and NO_x via investigating the effects of several input parameters, processes, and experimental conditions.

In the case of VOC decomposition, the effective removal of acetaldehyde by humidified air plasma was investigated with a high throughput of contaminated gas in a sandwiched honeycomb catalyst reactor at surrounding ambient temperature. Here, acetaldehyde at the level of a few ppm was successfully oxidized by the honeycomb plasma discharge despite the harsh condition of large water content in the feed gas. The conversion rate of acetaldehyde increased significantly with the presence of catalysts coating on the surface channels. The increased conversion rate was also obtained with a high specific energy input (SEI) and total flow rate. Interestingly, the conversion changed negligibly under the acetaldehyde concentration range from 5 to 20 ppm. However, the conversion rate decreased toward increased water amount in the feed gas. Notably, about 60% of acetaldehyde in the feed was oxidized under SEI of 40 J/L at water amounts $\leq 2.5\%$, approximately 0.5 g/kWh for acetaldehyde removal. Also, the plasma-catalyst reaction was superior to the thermal reactive catalyst for acetaldehyde removal in airborne pollutants. In comparison with other plasma-catalyst sources for acetaldehyde removal, the energy efficiency under the condition is comparable. Moreover, the honeycomb plasma discharge features high throughput, avoiding

pressure drop, and straightforward reactor configuration, suggesting potential practical applications.

The removal of NO_x over $\text{Ag}/\gamma\text{-Al}_2\text{O}_3$ catalyst coupled with gliding arc plasma at low temperatures is demonstrated. Specifically, *n*-heptane (the reducing agent) was pretreated by exposure to gliding arc plasma (the outlet gas temperature of 73.4 °C) before injecting into the simulated diesel exhaust gas and passing it through the catalyst zone. As a result of the plasma treatment, the feed gas consisted of oxygenated hydrocarbons (OHCs), which serve as reducing agents, instead of only *n*-heptane without plasma treatment. Consequently, the NO_x removal efficiency increased substantially by approximately 10% at temperatures of [165-225 °C], owing to the presence of the OHCs. The dependence of the NO_x removal efficiency on typical reducing agents was examined; these results agreed with our hypothesis that aldehyde derivatives were more effective than the parent compound (*n*-heptane) for NO_x removal at low temperatures. However, enhancement of the NO_x removal efficiency after plasma pretreatment was not observed at high plasma discharge power. This is because NO_x is formed from the air and a significant amount of *n*-heptane is completely oxidized to CO_2 when the gliding arc plasma is operated at high power. Besides, the plasma treatment of *n*-heptane did not improve the NO_x removal under high operating temperature conditions at which the catalyst itself exhibits high catalytic activity. This led us to surmise that boosting the effectiveness of the OHCs generated during plasma pretreatment would require the ratio of the exhaust gas flow rate to the reducing agent flow rate to be high, which is challenging to realize in laboratory-scale experiments. This method would lower the energy consumption of the plasma stage.

DECLARATION

I declare that the thesis entitled “**Development of Large Volume Air Plasma for Practical Application to Gas Contaminant Removal**” submitted to the Jeju National University, in partial fulfillment of the requirements for the award of the Degree of Doctor of Philosophy in the **Faculty of Applied Energy Systems, Major of Energy & Chemical Engineering** is a record of original and independent research work done and published by me during the period of September 2019 to August 2022 under the supervision and guidance of **Prof. Young Sun Mok**, Department of Chemical Engineering, Jeju National University. This thesis is solely based on our publication in reputed journals. It has not been submitted to any other Degree/ Diploma/ Associateship/ Fellowship to any candidate of any university.

Matyakubov Nosir Shihnazarovich

ACKNOWLEDGEMENTS

I would like to thank everyone that has contributed and supported the accomplishment of this work.

First of all, I would like to express my deepest gratitude and greatest appreciation to my supervisor, Prof. Young Sun Mok. Dear prof. Mok, thank you so much for giving me the opportunity of doing my Ph.D. in your research team. I am grateful for your permanent encouragement, guidance, support, and scientific advice and ideas in accomplishing this study. I learned many nice things from you that are momentous and helpful both in my research career and also in my life.

I would also like to express my sincere gratitude to Dr. Ulugbek Shaislamov and Dr. Bunyod Allaberganov for recommending me to this lab for the doctoral course. Without their help, I couldn't get such an excellent opportunity to work in this lab. I also thank them for their support and advice during my doctoral course and living in Korea.

I am grateful to Dr. Duc Ba Nguyen for his suggestions, support, and advice in performing experiments and publishing papers. He was very kind to help me with the basics of constructing experimental setups and controlling plasma systems. I always appreciated his support.

I extend my sincere thanks to the thesis evaluation director, Professor Lee Ho Won, and thesis committee members, Professor Heonju Lee, Professor Kim Sang Jae, and Professor Kim Woo Young, for their time, interest, excellent suggestions, and support in finishing my thesis.

I am especially thankful to my lab colleagues and friends, Dr. MSP Sudhakaran, Dr. Mokther, Dr. Kim, Dr. Siddiqi, Dr. Selvan, Dr. Toan, Mr. Roshan, Mrs. Shirjana, Mrs. Sosi, Mr. Yoon, and Mr. Avik for their warm friendship, support, and making the best environment in the lab. I had great pleasure working with you!

I am glad to have my Uzbek friends, Azimbek Khudoyberdiev and Nodirbek Kosimov, who are very supportive and made a homely environment while living in Korea.

I must thank the university administration for providing me with a full tuition fee waiver. I would like to thank the chemical engineering department personnel for their kindness and help in official issues. I also thank the BK21 plus fellowship program administration for providing me with sufficient funds for my living.

Last but certainly not least, I would like to express my deepest gratitude to my parents, Mr. Matyakubov Shixnazar and Mrs. Ibragimova Asiljan. They have dedicated their entire life to the betterment of our tomorrow with love and thankfulness. I also thank my brothers, Matyakubov Matyakub, Matyakubov Mansurbek, and Matyakubov Nodirbek, for their permanent support and help in my life. And my most enormous thanks to my wife for her support and understanding. For my kids, sorry for being even grumpier than normal whilst I wrote this thesis.

Words can hardly substitute the thankful that I owe to my inspiring teachers and friends who stood behind me in all possible ways to complete this work successfully. Without the above, I might not finish this research work as a great full one. I thank one and all who have helped me, directly and indirectly, to complete my research works.

Thanks & Regards

Matyakubov Nosir Shihnazarovich

TABLE OF CONTENTS

ABSTRACT	III
DECLARATION	V
ACKNOWLEDGEMENTS	VI
TABLE OF CONTENTS	1
LIST OF FIGURES	5
LIST OF TABLES	9
ABBREVIATIONS	10
CHAPTER 1 – INTRODUCTION TO THE RESEARCH	12
1.1. Background	13
1.2. Plasma	15
1.3. The environmental problems.....	18
1.3.1. Climate change and the greenhouse effect.....	18
1.3.2. Acid rain.....	19
1.3.3. Ozone layer depletion and Ground-level ozone.....	19
1.4. Research purpose	19
1.5. Structure of the dissertation	20

CHAPTER 2 – EXPERIMENTAL MATERIALS AND METHODS	22
2.1. Corona discharge plasma for acetaldehyde removal.....	22
2.1.1. Configuration of IPC reactor.....	22
2.1.2. Experimental setup.....	24
2.1.3. Term definition used for analyzing the result	26
2.2. Gliding arc plasma for NO _x removal	27
2.2.1. Configuration of PPC reactor.....	27
2.2.2. Catalyst preparation	29
2.2.3. Experimental setup.....	29
2.2.4. Properties of gliding arc plasma discharge	31
2.2.5. Term definition used for analyzing the result	34
 CHAPTER 3 – EFFECTIVE PRACTICAL REMOVAL OF ACETALDEHYDE BY A SANDWICH-TYPE PLASMA-IN-HONEYCOMB REACTOR UNDER SURROUNDING AMBIENT CONDITIONS	 36
3.1. Introduction	36
3.2. Experimental	36
3.3. Results and Discussion.....	36
3.3.1. Dependence of honeycomb discharge on acetaldehyde concentration and process time.....	36
3.3.2. A role of metal catalyst on the acetaldehyde removal process	40

3.3.3. Dependence of the acetaldehyde removal on the input parameters	45
3.3.4. Plasma chemistry of honeycomb discharge	51
3.3.5. Comparison of acetaldehyde removal by the honeycomb plasma with other processes	52
3.4. Summary	56
CHAPTER 4 – ENHANCING THE SELECTIVE CATALYTIC REDUCTION OF NO_x AT LOW TEMPERATURE BY PRETREATMENT OF HYDROCARBONS IN A GLIDING ARC PLASMA	57
4.1. Introduction	57
4.2. Experimental	58
4.3. Results and Discussion.....	58
4.3.1. Performance of NO _x removal over Ag/γ-Al ₂ O ₃ catalyst in the low-temperature range.....	58
4.3.2. Improvement of NO _x removal by gliding arc plasma	62
4.3.3. Potential pretreatment of HC injection by plasma and future study	69
4.3.4. Analysis of optical emission spectra of the gliding arc plasma	70
4.4. Summary	72
CHAPTER 5 – GENERAL CONCLUSION	73
BIBLIOGRAPHY	76

APPENDIX A: LIST OF PUBLICATIONS92

APPENDIX B: LIST OF CONFERENCES.....94

LIST OF FIGURES

Figure 2.1. Schematic diagram of the honeycomb corona discharge reactor.	23
Figure 2.2. Images of (a) bare and (b) catalyst monolith and (c) corona discharge in honeycomb catalyst.....	24
Figure 2.3. Schematic diagram of the experimental setup.....	25
Figure 2.4. Schematic diagram of PPC system (a) and schematic diagram of the gliding arc plasma reactor with dimensions (b).....	28
Figure 2.5. Images of the γ -Al ₂ O ₃ pellet (a) before and (b) after synthesizing 2 wt % of Ag.	29
Figure 2.6. Schematic diagram of the experimental setup.....	30
Figure 2.7. Electrical waveform of gliding arc plasma at input power of 11 W (a) voltage, (b) current, and (c) image of discharge (total flow rate of 2 L/min with N ₂ /O ₂ = 9/1; n-heptane _{inlet} = 2314 ppm).....	33
Figure 2.8. Gas temperature at the outlet of gliding arc plasma (input power = 11 W, total flow rate of 2 L/min with N ₂ /O ₂ = 9/1; n-heptane inlet = 2314 ppm).	34
Figure 3.1. <i>Effects of presence/absence of acetaldehyde on the discharge power and gas outlet temperature (Applied voltage = 20 kV; C₂H₄O inlet = 100 ppm; water content = 3.3%; total flow rate = 70 L/min).</i>	37
Figure 3.2. Comparison adsorbed acetaldehyde between the bare monolith and monolith catalyst under humidity of 2.5% (C ₂ H ₄ O inlet = 21 ppm; total flow rate = 40 L/min).	38

Figure 3.3. Evolution of the concentration of acetaldehyde and discharge power under applied voltage =15 kV and water amount of 2.5% (C ₂ H ₄ O inlet = 23 ppm; total flow rate = 40 L/min).	39
Figure 3.4. Evolution of the water amount during a honeycomb plasma discharge for removal of acetaldehyde (Applied voltage =15 kV; C ₂ H ₄ O inlet = 23ppm; total flow rate = 40 L/min).	40
Figure 3.5. Comparison between the bare monolith and monolith catalyst on the (a) discharge power, (b) curve of voltage and current discharge at 25 kV, and (c) conversion of acetaldehyde (total flow rate = 60 L/min; water content = 2.5%; C ₂ H ₄ O inlet = 5 ppm).	42
Figure 3.6. (a) effects of flow rate on the removal of acetaldehyde with inlet acetaldehyde fixed at 5 ppm and (b) formation of O ₃ at SEI of 25 J/L under the absence of acetaldehyde (water content = 2.5 %).	46
Figure 3.7. Effects of water amount in the feed gas on the (a) discharge power, (b) capacitor and resistance under without plasma discharge (the reactor was unconnected with plasma power supply), and (c) removal of acetaldehyde (C ₂ H ₄ O inlet = 5 ppm; total flow rate = 60 L/min).	49
Figure 3.8. Effects of initial concentration of acetaldehyde on the conversion rate (total flow rate = 60 L/min; water amount =2.5%; SEI = 55 J/L).	51
Figure 3.9. Optical emission spectrum at 2-mm discharge gap of high-voltage electrode and monolith catalyst at SEI of 40 J/L (total flow rate = 60 L/min; water amount =2.5%; SEI = 40 J/L; C ₂ H ₄ O inlet = 5 ppm).	52

Figure 3.10. A Comparison between thermal catalytic activity and plasma for acetaldehyde conversion based SEI consumption (GHSV = 10,600 h ⁻¹ ; water amount =2.5%; C ₂ H ₄ O inlet = 5 ppm).....	54
Figure 4.1. Dependence of NO _x conversion on reducing agent at different temperatures (GHSV=5000 h ⁻¹ ; NO _{inlet} =300 ppm; C ₁ /N = 6; water content = 1.7 %; total flow rate = 12 L/min).....	58
Figure 4.2. Effect of C ₁ /N ratio on the NO _x conversion under n-heptane as the reducing agent at 252°C (GHSV=5000 h ⁻¹ ; NO _{inlet} =300 ppm; water content = 1.7 %; total flow rate = 12 L/min).....	60
Figure 4.3. Effect of the water content of the feed gas on the removal efficiency of NO _x at 252 °C (total flow rate = 12 L/min; NO _{inlet} =300 ppm and n-heptane as reducing agent with C/N=9).....	62
Figure 4.4. Enhancing the removal efficiency of NO _x at low temperatures by coupling the catalytic removal process with gliding arc plasma to generate oxygenated hydrocarbons from n-heptane (GHSV=5000 h ⁻¹ ; NO _{inlet} =300 ppm; n-heptane _{inlet} =386 ppm; water content=3.5 %; total flow rate=12 L/min in which 2 L/min with O ₂ /N ₂ =1/9 for plasma; input power ~ 11 W; SEI of 55 J/L).....	64
Figure 4.5. Chromatograms of gases produced in the gliding arc reactor at ~ 11 W input power (Flow rate of 2 L/min: O ₂ /N ₂ =1/9; n-heptane _{inlet} =2314 ppm that equilibrium to 386 ppm after diluting to 12 L/min).....	65
Figure 4.6. Effect of the input power on the removal efficiency of NO _x when the catalyst is operated at 223 °C (GHSV=5000 h ⁻¹ ; NO _{inlet} =300 ppm; n-heptane _{inlet} =386	

ppm; water content=3.5 %; total flow rate=12 L/min in which 2 L/min with O₂/N₂ =1/9 for plasma). 66

Figure 4.7. Effects of input power on the (a) formation of NO_x and (b) conversion of n-heptane and formation of CO₂ using gliding arc plasma (plasma flow rate = 2 L/min with O₂/N₂ =1/9 and concentration of n-heptane = 2314 ppm; CO₂ and NO_x concentration were measured after diluting to 12 L/min)..... 68

Figure 4.8. Comparison between the removal efficiency and absolute amount of NO_x reduced (GHSV = 5000 h⁻¹; NO_{inlet} = 300 ppm; n-heptane_{inlet} = 386 ppm; water content = 3.5 %; total flow rate = 12 L/min in which 2 L/min with O₂/N₂ =1/9 for plasma; SIE = 55 J/L)..... 70

Figure 4.9. Optical emission spectra of gliding arc plasma at ED of 330 J/L (—, blue line) with n-heptane = 2314 ppm in the feed gas and (—, red line) without n-heptane in the feed gas (plasma flow rate = 2 L/min in with O₂/N₂ =1/9)..... 71

LIST OF TABLES

Table 1.1. The main chemical reactions that occur in plasmas. These data are taken from [36]	16
Table 1.2. Characterizations of the kinds of plasma	18
Table 3.1. A comparison between several plasma-catalyst systems for acetaldehyde removal process under atmospheric pressure conditions.....	55

ABBREVIATIONS

AC	Alternating current
Ag	Silver
AgNO ₃	Silver nitrate
Al ₂ O ₃	Alumina Oxide
°C	Degree celsius
C ₂ H ₄ O	Acetaldehyde
C ₇ H ₁₆	n-Heptane
CO	Carbon monoxide
Co	Cobalt
CO ₂	Carbon dioxide
DBD	Dielectric barrier discharge
e	Electron
ED	Energy density
eV	Electron-Volt
FTIR	Fourier transforms infrared
GA	Gliding Arc
GC	Gas Chromatography
GHSV	Gas Hourly Space Velocity
H ₂	Hydrogen
HC	Hydrocarbon
HC-SCR	Hydrocarbon Selective Catalytic Reduction
HV	High Voltage

Hz	Hertz
H ₂ O	Water vapor
ID	Inner diameter
IPC	In Plasma Catalyst
K	Kelvin
kJ	Kilojoule
kΩ	Kiloohm
L	Liter
La	Lanthanum
M	Molecule
MΩ	Megaohm
MFC	Mass Flow Controller
MgO	Magnesium oxide
mm	Millimeter
min	Minute
η	Removal efficiency
N ₂	Nitrogen
NH ₃	Ammonia
NO	Nitrogen oxide
NO ₂	Nitrogen dioxide
NO _x	Nitrogen oxides
NTP	Non-Thermal Plasma
O ₂	Oxygen

O ₃	Ozone
OD	Outer diameter
OES	Optical Emission Spectroscopy
OHC	Oxygenated Hydrocarbon
OH	Hydroxide
Pd	Palladium
pF	Pikofarad
ppm	Parts per million
PPC	Post Plasma Catalyst
Pt	Platinum
RH	Relative humidity
s	Second
SiO ₂	Silicon dioxide
SCR	Selective Catalytic Reduction
SEI	Specific Energy Input
VOC	Volatile Organic Compound

CHAPTER 1 – INTRODUCTION TO THE RESEARCH

1.1. Background

Reducing emissions of air pollutants such as volatile organic compounds (VOC) and nitrogen oxides (NO_x) have been interesting and important research due to their harmful impact on the environment and human health. Power plants, industry, and transportation, which take energy by burning fossil fuels, are NO_x's primary outer sources [1-3]. Moreover, indoor sources of VOCs, including carpet, wallpapers, furniture, and tiles [4-8], are a severe issue to people's health because most people spend their time at the home, office, school, etc. [9, 10]. Currently, diesel engines are still the primary sources of power for heavy-duty vehicles, marine engines, and power plants [11, 12], and the use of diesel fuel gives rise to the emission of NO_x [12, 13]. Consequently, the manufacturers of diesel engines are under pressure to lower the emissions of pollutants caused by diesel to comply with standard requirements [13, 14]. Also, with rapidly increasing industrialization and population worldwide, more energy should be generated to provide for all the areas. Up to date, it is impossible to change all of these sources to renewable energy sources because of the limitation of generating renewable energy [13, 15, 16]. As a result, reducing emissions from the sources is a considerable problem to solve on a large scale to improve the planet's air quality.

Various technologies have been implemented to control emissions of VOCs and NO_x. For example, for removal of VOC, ultraviolet oxidation, biofiltration, membrane filtration, adsorption and absorption, thermal and catalytic oxidation [3, 17-23] are used as conventional methods. In the case of NO_x reduction, urea-selective catalytic reduction or active lean NO_x catalysts have been widely used [18]. In the hydrocarbon selective catalytic reduction (HC-SCR) of NO_x, diesel fuel serves as the reducing agent, and the use of another reducing agent such as NH₃ or urea is not required [24-26]. The removal of NO_x via HC-SCR is highly efficient in the temperature range from 250 to 350 °C [27-30]. However, its efficiency

decreases sharply at lower temperatures of 180–250 °C because the activity of the catalyst is lower in this temperature range [31]. Nevertheless, the adsorption and absorption techniques have some disadvantages; for example, reactivating/post-treatment and disposal of the used adsorbents may increase the overall cost [23, 32]. Similarly, high temperature is required for thermal and catalytic oxidation technologies, and the use of some catalysts in real conditions is limited due to the high cost of catalytic materials [23, 33]. Alternative air purification methods are nonthermal plasma (NTP), and NTP-assisted catalyst hybrid systems are considered perspective methods to increase energy efficiency [18, 22, 34, 35]. However, the use of the NTP system for removing NO_x or VOC has some drawbacks because of the incomplete decomposition, low energy efficiency, production of hazardous by-products such as CO, NO_x, and new VOCs [36].

Among these technologies, the nonthermal plasma catalytic hybrid method is one of the best promising and attractive techniques for reducing emissions at atmospheric pressure and low temperature with low energy consumption [36-42].

A dielectric barrier discharge (DBD) reactor is a common NTP that has been used widely in VOC as well as acetaldehyde removal [43, 44]. The DBD has a simple plasma system design and stable plasma discharge with current extinguishing on the surface of the dielectric layer between two electrodes. Moreover, there is a synergetic effect of plasma coupled with a catalyst for VOC removal [45]. As a result, a packed-bed DBD is frequently used to investigate VOC removal [43]. Although a packed-bed DBD successfully removes VOC, the system is limited to high flow rates due to high-pressure drop. An alternative approach to addressing this issue is the production of plasma in a honeycomb-structured catalyst [46]. Several configurations have been useful for the generation of honeycomb discharge, including DBD, corona discharge, and ignition plasma discharge, along with back corona discharge [47]; unfortunately, there is still a constraint on the size of the honeycomb (≤ 30 mm) [48]. Among

these plasma configurations, the generation of plasma in a honeycomb with a sandwich-type honeycomb plasma reactor is simple, capable of operating with a large honeycomb size, and facilitates practical applications. Indeed, the configuration consists of a honeycomb catalyst that is sandwiched in two parallel electrodes [49-55]. Recently, a humidified air plasma inside a commercial honeycomb monolith with a diameter of 93 mm and a length of 50 mm was successfully produced by a sandwich reactor [48]; in addition, the plasma discharge is highly dependent on the amount of water in the feed gas. Fortunately, this condition is similar to actual indoor emissions of VOCs; the water amount can be dependent on the surrounding ambient conditions.

Enhancing the removal efficiency of NO_x by the pretreatment of hydrocarbons (HC) with plasma to generate OHCs is another promising technology for practical plasma applications. The technical key is that OHCs would be more effective than the original HCs for the HC-SCR process in the low-temperature range [56, 57]. The HC flow injection could be adjusted to form a predetermined fraction of the diesel exhaust gases, at a few liters per min, suggesting that practical application would be feasible. A dielectric barrier discharge (DBD) features stable plasma at atmospheric pressure and a low current of a few milli-ampere [58]; however, a large discharge volume is required even though the flow rate is a few liters per min. In contrast, a small gliding arc (GA) plasma is still able to operate at a high flow rate and supply high current discharge (at the ampere level)[59] because the two electrodes are not isolated with a dielectric layer. These advantageous features of GA plasma mean that they are potentially useful for oxidizing HCs to form OHCs before injecting diesel exhaust gases for NO_x removal.

1.2. Plasma

Plasma is referred to as the fourth state of matter and can be made on a lab-scale, in industry, and naturally [37, 60, 61]. Plasma can be generated by supplying a high voltage

electric field or thermal energy to gas or matter and creates from entirely to weakly ionized gas consisting of energetic electrons, reactive species, atoms, and ions. Moreover, plasma technology has been a promising method in various fields, such as materials processing, environmental control, lasers, medicine, and energy systems [62-66]. Based on the temperature and density of energetic electrons and gases, plasma can be classified into several types, such as thermal (hot) and nonthermal (cold) plasma. In producing nonthermal plasma, most electric energy (>99%) can be transferred to generate energetic electrons instead of heating the whole gas flow. These energetic electrons can form ions, excited species, free radicals, and additional electrons due to electron impact ionization, dissociation, and excitation of gas molecules [37, 60, 65]. The possible chemical reactions in plasmas are shown in Table 1.1.

Table 1.1. The main chemical reactions that occur in plasmas. These data are taken from [36]

Electron/molecular reactions	
Excitation	$e^- + A_2 \rightarrow A_2^* + e^-$
Dissociation	$e^- + A_2 \rightarrow 2A + e^-$
Attachment	$e^- + A_2 \rightarrow A_2^-$
Dissociative attachment	$e^- + A_2 \rightarrow A^- + A$
Ionization	$e^- + A_2 \rightarrow A_2^+ + 2e^-$
Dissociative ionization	$e^- + A_2 \rightarrow A^+ + A + e^-$
Recombination	$e^- + A_2^+ \rightarrow A_2$
Detachment	$e^- + A_2^- \rightarrow A_2 + 2e^-$
Atomic/molecular reactions	

Penning dissociation	$M + A_2 \rightarrow 2A + M$
Penning ionization	$M^* + A_2 \rightarrow A_2^* + M + e^-$
Charge transfer	$A^\pm + B \rightarrow B^\pm + A$
Ion recombination	$A^- + B^+ \rightarrow AB$
Neutral recombination	$A + B + M \rightarrow AB + M$
Decomposition	
Electronic	$e^- + AB \rightarrow A + B + e^-$
Atomic	$A^* + B_2 \rightarrow AB + B$
Synthesis	
Electronic	$e^- + A \rightarrow A^* + e^-, \quad A^* + B \rightarrow AB$
Atomic	$A + B \rightarrow AB$

Here, A and B are atoms, A₂ and B₂ are molecules, e is an electron, M is a temporary collision partner, + and – indicate ions with their respective charge symbols, and * indicates an excited or radical species.

The temperature of energetic electrons ($\leq 10^5$ K) is much higher than the ion (gas) temperature as well as partially ionized, and the gas temperature is close to room temperature in non-equilibrium plasma. The gas components are fully ionized, and the temperatures of energetic electrons, ions, and radicals are equal in thermal and high-temperature plasma. In Table 1.2, the characteristics of kinds of plasmas are demonstrated [67-70].

Table 1.2. Characterizations of the kinds of plasma

	Nonthermal Plasma (non-equilibrium plasma)	Thermal Plasma (local equilibrium plasma)	High-temperature plasma (equilibrium plasma)
Temperature	$T_e \gg T_i$ $T_e \leq 10^5 \text{ K } (\approx 10 \text{ eV})$ $T_i \approx T_g \approx 300\text{-}10^3 \text{ K}$	$T_e \approx T_i \approx T_g$ $\leq 2 \cdot 10^4 \text{ K}$	$T_e \approx T_i \approx T_g$ $\approx 10^6\text{-}10^8 \text{ K}$
Ionization degree (a_i)	Weakly ionized ($10^{-6} < a_i < 10^{-1}$)	Fully ionized ($a_i \approx 1$)	Fully ionized ($a_i \approx 1$)
Electron density	$< 10^{19} \text{ m}^{-3}$	$\approx 10^{21}\text{-}10^{26} \text{ m}^{-3}$	$\geq 10^{20} \text{ m}^{-3}$
Examples	Corona, glow, arc discharge, and wave heated plasma.	Arc plasma, plasma torches	Fusion Plasmas, Kinetic plasmas
Applications	Environmental control, biomedicine, textile technology	Welding, cutting, spraying	Semiconductor manufacturing, melting

Ionization degree - (a_i), Electron temperature - T_e , Ion temperature - T_i , Gas temperature - T_g .

This study used corona discharge plasma in a honeycomb monolith and gliding arc plasma for VOC decomposition and NO_x reduction.

1.3. The environmental problems

1.3.1. Climate change and the greenhouse effect

Long-term shifts in weather patterns and temperature have been referred to as climate change. Climate change is caused by global warming and its effects on the environment. Instead, the emissions of greenhouse gases from human activity, transportation, power plants are the main reasons for an increase in the weather temperature of the atmosphere [71-73]. Carbon dioxide (CO_2), methane (CH_4), nitrous oxide (N_2O), nitrogen oxides (NO and NO_2),

ozone (O_3), and water vapor (H_2O) are the main gases that lead to global warming and the greenhouse effect.

1.3.2. Acid rain

Depositions of oxides on the planet's surface by acidified rain are also known as acid rain. Acid rain can be harmful effects on human health, growing plants, forests, freshwater, soil, animals, and infrastructure. The primary acid sources are emissions of air pollutant gases such as nitrogen oxides (NO_x) and sulfur oxides (SO_x) from combustion engines of power plants, transportations, and industry. Reducing these emissions plays a vital role in environmental issues [71-73].

1.3.3. Ozone layer depletion and Ground-level ozone

The ozone layer is a thin region of the stratosphere and plays a crucial role in absorbing most ultraviolet radiations of the sun. Ozone layer depletion leads to increased ultraviolet radiation entering the atmosphere and changes the earth's ecosystems [74]. Ozone (O_3) is a colorless gas, and its formation in the troposphere (low-level of the atmosphere of the planet) is the most critical issue due to its hazardous impact on human health and the environment. VOCs and NO_x emissions on sunny days can increase the formation of ground-level ozone because of their photochemical reaction [75].

1.4. Research purpose

The overall research aim of this thesis is to develop the NTP catalyst systems for environmental control that increase the removal efficiency of VOC (acetaldehyde) and NO_x . In plasma catalyst (IPC) reactor for acetaldehyde removal and a post-plasma catalyst (PPC) system for NO_x reduction are examined. The acetaldehyde is successfully decomposed on a practical scale by the corona discharge in the commercial honeycomb monolith catalyst. The PPC reactor was implemented to enhance NO_x removal efficiency over the $Ag/\gamma-Al_2O_3$ catalyst from diesel exhaust gas at low temperatures.

Several vital points as objectives of the thesis:

- Investigate the influence of various input parameters and conditions, including the water content of the feed gas, total gas flow rate, absence/presence of metal on the honeycomb monolith, input energy, inlet concentration of acetaldehyde, and process time on the acetaldehyde conversion.
- Investigate comparing the thermal process and the NTP catalyst for acetaldehyde conversion.
- Investigate the generation and parameters of gliding arc plasma for reforming HC to OHCs.
- Investigate the effects of reducing agents, C₁/N ratio, the humidity of the feed gas, and input power on the NO_x reduction over the Ag/ γ -Al₂O₃ catalyst.

1.5. Structure of the dissertation

The structure of this thesis is organized as follows.

Chapter 1 presents literature overviews on environmental control and several causes and sources of the problems and methods that have been used for air pollution control. Thus, various advantages and disadvantages of conventional technologies and alternatives are introduced. The chapter contains a brief introduction to plasma, including classifications and applications and the study's objectives.

In chapter 2, the experimental methodologies of the research are described in detail. Types of plasma reactors, their design, preparation of catalysts, and experimental setups used in this work are shown. Moreover, methods for calculations and analysis of electrical parameters and definitions are also reported.

In chapter 3, the application of nonthermal plasma in honeycomb monolith catalyst for acetaldehyde removal is investigated. Furthermore, the chapter consists of experimental

results and discussion, for instance, the dependence of several inlet parameters and conditions on acetaldehyde conversion. In addition, the chapter reports the plasma chemistry of honeycomb discharge, comparison removal of acetaldehyde in different processes, and a summary of the work.

Chapter 4 reports the investigation of NO_x reduction over the $\text{Ag}/\gamma\text{-Al}_2\text{O}_3$ catalyst by injection method from the diesel exhaust gas. Notably, this chapter discusses various properties of gliding arc plasma and the effects of gliding arc plasma in different conditions on NO_x removal. Also, the chapter gives an analysis of the optical emission spectra of the gliding arc plasma and a summary of the study.

Chapter 5 presents several vital research findings as the conclusions of the research.

CHAPTER 2 – EXPERIMENTAL MATERIALS AND METHODS

This chapter presents the configuration of nonthermal plasma reactors and experimental setups, including honeycomb corona discharge plasma reactor for VOC removal and gliding arc plasma reactor for removal of NO_x. This chapter also describes and discusses the controlling methods of plasma systems, measurement, and analyzing parameters.

2.1. Corona discharge plasma for acetaldehyde removal

2.1.1. Configuration of IPC reactor

Corona plasma is a kind of gas discharge that appears at atmospheric pressure because of the large electric field near sharp points of the electrode; hence the design and geometry of the electrode play a vital role in the generation of corona discharge [36, 37, 76]. In corona discharge, the strength of the electric field is superior to the equivalent constant discharge at a similar current, and chemical bonds can be destroyed by energetic electrons and produce free radicals; as a result, a nonthermal chemical reaction can occur [35, 70, 77]. Corona discharges are a more effective technique for gas purifications and VOC removal because of the large discharge volume, high-energy efficiency, and low operating costs [36, 60, 62, 76, 78, 79].

In plasma catalyst reactor is used for acetaldehyde decomposition on a practical scale. The corona discharge in a honeycomb monolith is successfully generated with humidified high airflow at atmospheric pressure and room temperature. The configuration of the IPC reactor is shown in Figure 2.1. The plasma is based on AC discharge and generated in the zone created by two parallel stainless-steel perforated disks (168 holes; diameter hole of 3 mm; a discharge gap of 52 mm). The commercial honeycomb (93-mm diameter, 50-mm length, 300 cpsi) located inside the gap with the honeycomb touched the ground electrode. The catalyst was produced by Ceracomb Co., Ltd., Korea. The metal catalyst composition of the monolith was examined by an inductively coupled plasma atomic emission spectrophotometer (5100 ICP-OES, Agilent, USA). The result presented that the surface of honeycomb channels consisted

of La, Pt, Pd, and Co with 0.03, 0.03, 0.07, and 0.10 wt.%, respectively, based on a total monolith weight of ~ 260g. In Figure 2.2, images of the bare honeycomb (a), metal-coated honeycomb catalyst (b), and corona discharge in the honeycomb catalyst are presented. The image of corona discharge plasma is taken under the condition (flow rate = 60 L/min; applied voltage $V_{p-p} = 55$ kV; discharge power = 40 W; water content = 2.5 %).

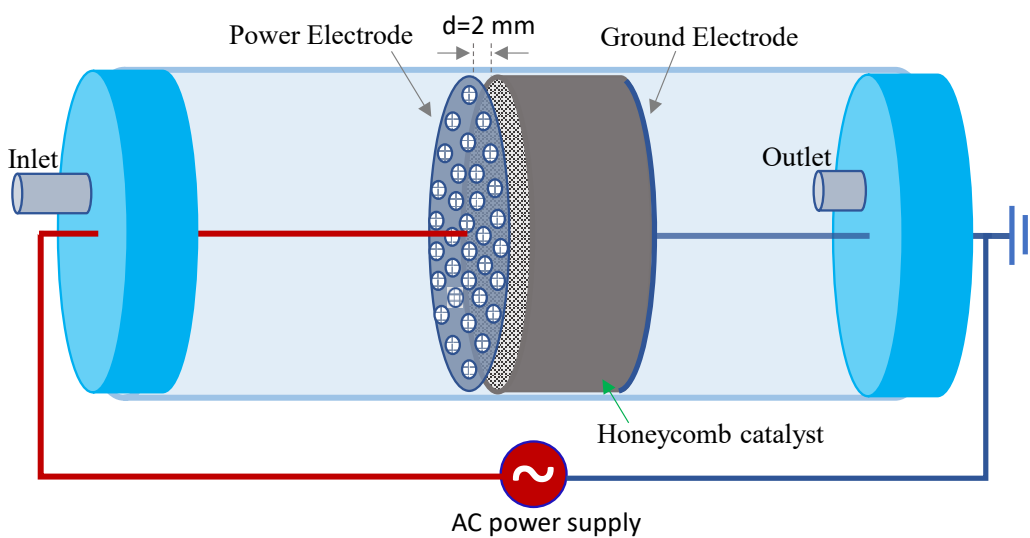


Figure 2.1. Schematic diagram of the honeycomb corona discharge reactor.

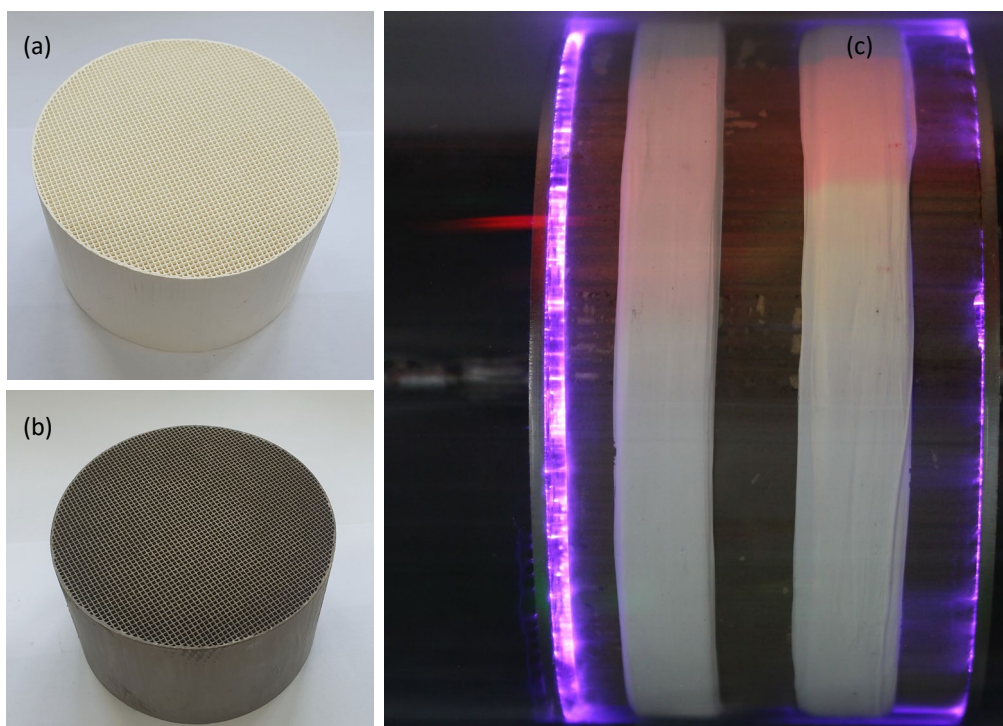


Figure 2.2. Images of (a) bare and (b) catalyst monolith and (c) corona discharge in honeycomb catalyst.

2.1.2. Experimental setup

The decomposition of acetaldehyde was investigated by a giant plasma volume of humidified air under surrounding ambient conditions. The humidified air plasma produced in a honeycomb-type monolith plasma reactor with an experimental setup is shown in Figure 2.3.

The feed gas was a mixture of acetaldehyde with a large volume of moisture air. The flow rate of acetaldehyde was controlled via an N_2 flow through the Erlenmeyer flask containing acetaldehyde, kept in a water bath at 5 °C. Individually, 7.1 ml/min N_2 flow through the Erlenmeyer flask was introduced by a mass flow controller (AFC500, Atovac Co., Korea); subsequently, the mixture of N_2 and acetaldehyde was diluted with another 86 ml/min N_2 , first-time dilution. To obtain 5 ppm acetaldehyde, the 4 ml/min of first-time diluted acetaldehyde mixture was incorporated with 60 L/min humid air, the second-time dilution.

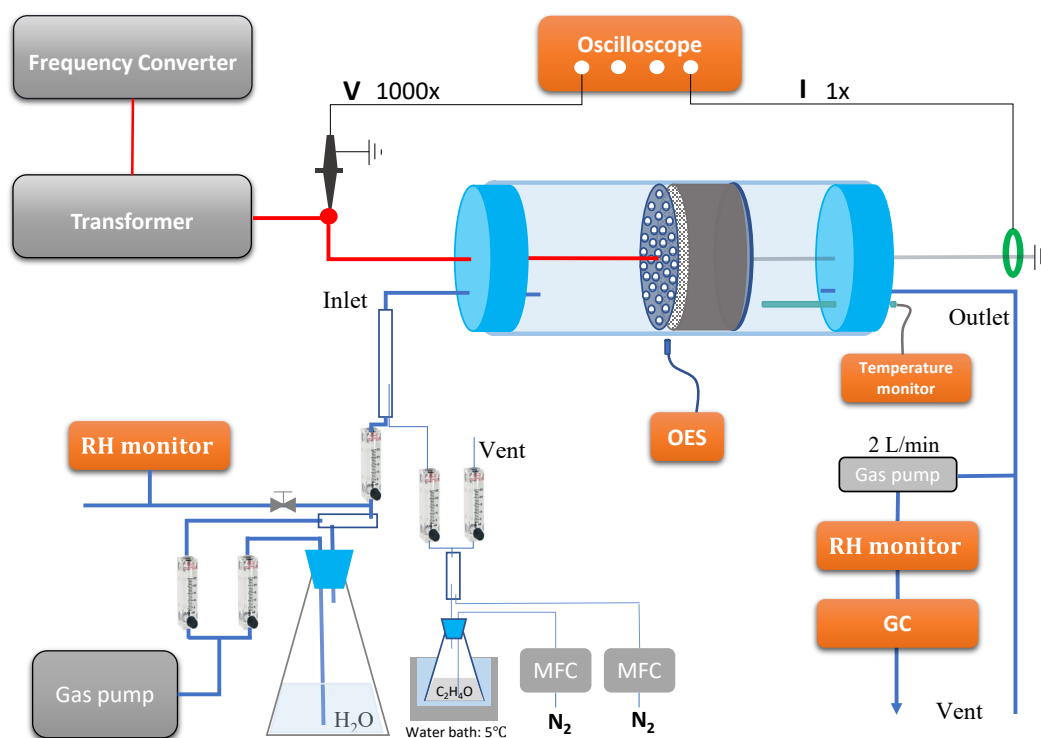


Figure 2.3. Schematic diagram of the experimental setup.

The humidified airflow rates were controlled by ball flowmeters (Dwyer, RMA-25-SSV, USA). Furthermore, the absolute humidity of water vapor was regulated by the dry-air part mixed with the remained humidified air. The absolute water vapor was calculated via temperature and relative humidity (RH); these parameters were measured by a humidity meter (TES Electrical Electronic Corp., TES-1370 NDIR CO₂ Meter, Taiwan). In this study, the water amount was examined up to 3.3%, corresponding to RH 100% at 26 °C; the range is similar to the water level in the indoor emission.

The contaminated air plasma was ignited and sustained by 400-Hz AC high voltage from a high-voltage transformer (Tae Hwa Electric Co., Korea); the primary voltage up to 300V was provided by a frequency converter (Sampoong Power Co., Ltd., Korea). During plasma discharge, electrical parameters were recorded by a digital oscilloscope (Tektronix, DPO 3034, USA). The oscilloscope was installed with a high voltage probe (P6015A, Tektronix, USA)

and a current monitor (2100, Pearson Electronics, USA) used for the measurement of applied high voltage and total current, respectively. Here, it should be noted that the waveforms were acquired with the average mode of 8 samples by the oscilloscope setting.

The acetaldehyde, CO₂, and O₃ components in the gas outlet were analyzed with several types of equipment. Briefly, the concentration of acetaldehyde was determined by a gas chromatography (GC, Bruker 450-GC, USA). The O₃ concentration in the gas outlet was indicated with gas detector tubes (No.18M Ozone, 4-400ppm, GASTEC Corp., Japan). Furthermore, light emission from plasma discharge was recorded with an optical emission spectrometer (OES, AvaSpec-2048 XL, Netherlands). The temperature of the gas outlet was monitored with a copper thermal sensor. The thermal sensor was located inside the reactor at 30-mm and 10-mm distance from the center axis and ground electrode, respectively. Since the monolith is 93-mm in diameter, it should be mentioned that the temperature measurement is a representation of a positioned temperature, not the average temperature for the gas outlet.

2.1.3. Term definition used for analyzing the result

Plasma discharge dissipated to the honeycomb catalyst was calculated by integrating instantaneous voltage and current, as shown in Eq. 2.1.3.1. Furthermore, other parameters used for analysis, i.e., specific energy input (SEI), removal efficiency (conversion, η) of acetaldehyde, and an equivalent SEI, are also defined.

$$\text{Discharge Power, } P(W) = \frac{1}{T} \int_0^T P_{\text{instantaneous}} dt = \frac{1}{T} \int_0^T V(t)I(t) dt \quad (2.1.3.1)$$

$$\text{Specific Energy Input, SEI } \left(\frac{J}{L}\right) = \frac{P(W)}{Q(L/min)} \times 60 \quad (2.1.3.2)$$

$$\text{Removal Efficiency, } \eta (\%) = \frac{\text{Weight of } C_2H_4O \text{ conversion}}{\text{Weight of } C_2H_4O \text{ inlet}} = \left[1 - \frac{C_{\text{outlet}}}{C_{\text{inlet}}}\right] C_2H_4O \times 100$$

(2.1.3.3)

$$\text{Energy Efficiency, EE (g/kWh)} = \frac{\text{Weight of } C_2H_4O \text{ conversion (g)}}{\text{Energy consumption (kWh)}} = \frac{3.6 \times 44.05 \times C_{\text{inlet}} \times \eta}{24.45 \times SEI}$$

(2.1.3.4)

Where: $C_{\text{inlet/outlet}}$ (ppm) is the concentration of acetaldehyde (CH_3CHO) in the gas inlet/outlet; 1 mol of acetaldehyde has a weight 44.05 g; 1 mol of gas under atmosphere and at 25°C (298 K) has a volume of 24.45 L; 3.6 is a factor to obtain g/kWh with concentration unit as ppm in the Eq. 2.1.3.4. The equivalent SEI of the thermal catalyst process was estimated through input energy for heating air from room temperature (25°C) to the operating temperature, adopted from elsewhere [80].

$$\text{Equivalent SEI} \left(\frac{\text{J}}{\text{L}} \right) = \frac{1}{24,450} \left(C1 T + C2 C3 \coth \left(\frac{C3}{T} \right) - C4 C5 \tanh \left(\frac{C5}{T} \right) \right) \Big|_{T1}^{T2}$$

(2.1.3.5)

Where: $T1$ is 298 K (initial gas temperature, 25°C); $T2$ is operating temperatures; 24,450 is a constant for calculating equivalent SEI based on gas volume at 25°C , $C1 = 28958$, $C2 = 9390$, $C3 = 3012$, $C4 = 7580$, and $C5 = 1484$.

2.2. Gliding arc plasma for NO_x removal

2.2.1. Configuration of PPC reactor

The gliding arc plasma reactor is combined with $\text{Ag}/\gamma\text{-Al}_2\text{O}_3$ catalyst and used for NO_x reduction from the diesel exhaust gas at atmospheric pressure. The schematic diagram of the system is demonstrated in Figure 2.4(a). Gliding arc discharge can be generated by supplying an electric field between two diverging electrodes with the gas flow at atmospheric pressure and room temperature. The plasma discharge starts at the slightest gap between the electrodes, and the gliding arc moves with the gas stream to the broadest gap distance between the electrodes. Gliding arc plasma reactors can be operated by supplying AC or DC power on a practical scale [35, 36, 66, 81-85]. The gliding arc plasmas are considered a promising technology due to their low energy consumption compared with conventional methods and have been widely used for several applications, such as the decomposition of pollutants,

chemical reactions, CO₂ conversion, methane reforming, and hydrogen production [36, 84, 86-93].

The gliding arc plasma reactor is illustrated with dimensions in Figure 2.4(b). The GA reactor comprised an internal cone-shaped aluminum electrode (active length=23 mm, angle = 5°) connected to a high-voltage output of a transformer (Model: DKNE-18, Korea) of which the primary voltage was received from an AC-based power supply (SAM PONG POWER Co. Ltd., Korea). The stainless-steel tube (ID = 11 mm) served as the ground electrode. A rotating gliding arc was generated by supplying 60-Hz high voltage across the electrodes with tangential gas flow.

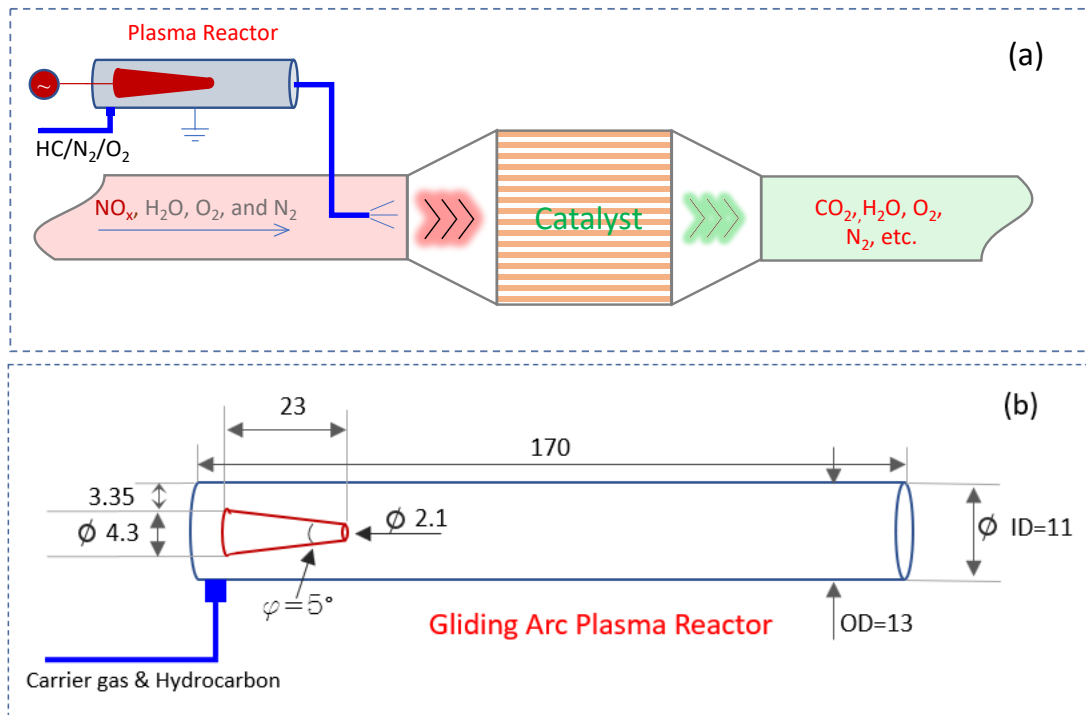


Figure 2.4. Schematic diagram of PPC system (a) and schematic diagram of the gliding arc plasma reactor with dimensions (b).

2.2.2. Catalyst preparation

The incipient wetness impregnation method was employed for synthesizing the catalyst Ag/ γ -Al₂O₃. Specifically, 200 g of Al₂O₃ pellets (size: 5 × 5 mm, Product code: 620100, Sasol, Germany) were impregnated with AgNO₃ solution (94.5 mL) containing 4.1 g of Ag. Figure 2.5 is demonstrated the images of the γ -Al₂O₃ catalysts before and after impregnation with silver. After 2 h, the impregnated pellets were exposed to the surrounding environment. Then, the sample was dried and calcined in a furnace (Model: SH-FU-80STG, SH SCIENTIFIC CO., Ltd, Korea) using a preprogrammed sequence. During the drying process, the temperature was increased from 25 to 110 °C at a rate of 3°C/min and kept constant at 110 °C for 3 h; for calcination, the temperature was increased from 110 to 550 °C at a rate of 5°C/min and then calcined for 6 h at 550°C. Thus, an Ag/ γ -Al₂O₃ catalyst containing 2.0 wt.% silver was prepared and used in the experiments to investigate the NO_x removal.

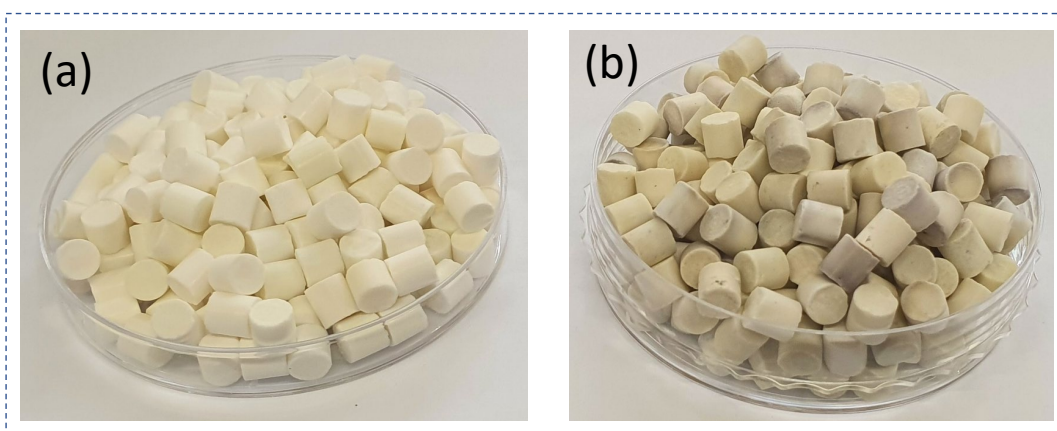


Figure 2.5. Images of the γ -Al₂O₃ pellet (a) before and (b) after synthesizing 2 wt % of Ag.

2.2.3. Experimental setup

Figure 2.6 shows a schematic diagram of the experimental setup that was used for NO_x reduction. The plasma catalyst system consisted of a gliding arc (GA) plasma reactor, a pre-heating system, and the Ag/ γ -Al₂O₃ catalyst was placed in a quartz tube (inner diameter, ID = 30 mm) in the furnace (Model: SH-FU-80STG, SH SCIENTIFIC Co., Ltd., Korea). The

system therefore consisted of two stages: the first entailed the successful reformation of HCs to OHCs in the GA reactor, and the second stage involved exposure of the gas to the catalyst at a temperature from 150 to 350 °C to perform NO_x removal. A digital oscilloscope (Tektronix, DPO 3034, USA) was used to record the voltage and current waveforms of the arc plasma. Specifically, the high voltage was measured by a passive high-voltage probe (Tektronix, P6015A, USA), whereas the current was determined by

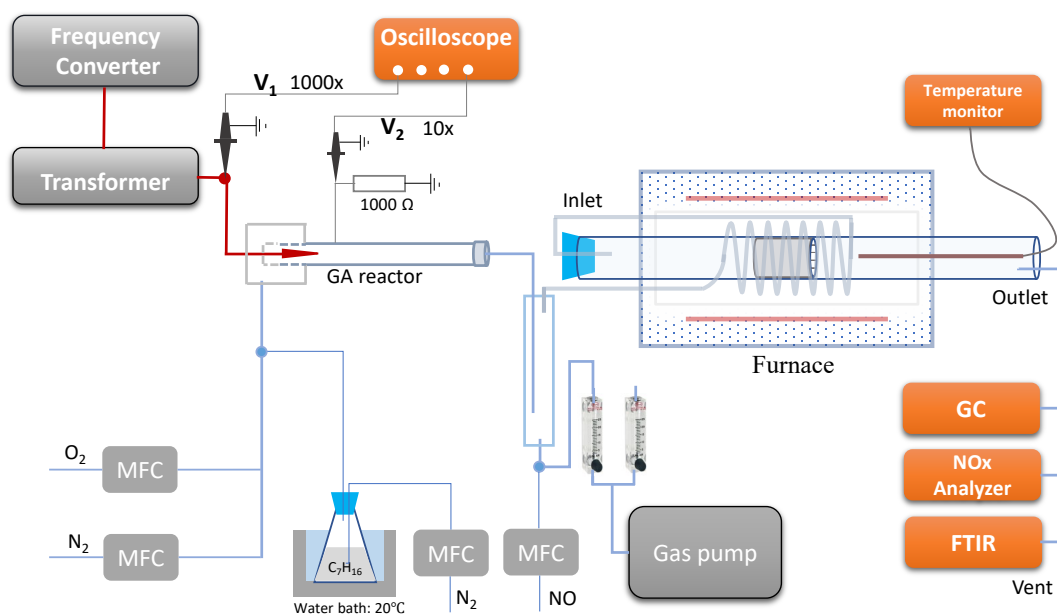


Figure 2.6. Schematic diagram of the experimental setup.

measuring the voltage across the 1 k Ω resistor, which was connected in series with the GA reactor, by a low-voltage probe (Tektronix, TPP0101, USA). Additional details of the relevant electrical parameters are provided in the following sub-section. The gas mixture that was fed into the GA reactor consisted of 10 % O₂ and 90 % N₂ in all the experiments. The gas flow rate through the GA reactor was maintained constant at 2 L/min. In addition, *n*-heptane was injected into the inlet of the GA reactor in a vaporized form in a stream of N₂, which was bubbled through the flask containing the liquid *n*-heptane maintained in a water bath at 20 °C. The total flow rate at the catalytic reactor was 12 L/min, including the gas flowing from the

outlet of the GA reactor at 2 L/min and air that contains NO flowing at 10 L/min. These two flows were mixed in a box, after which they were preheated by passing through a coiled stainless-steel tube before exposure to the catalyst. The respective flow rates of the N₂ and NO streams were each controlled by a mass flow controller (AFC500, Atovac Co., Korea). Ball flow meters (Dwyer, RMA-25-SSV, USA) were used for controlling the air flow rate, with the amount of water in the feed gas adjusted by passing part of the air flow through a water bottle or silica gel beads. A gas analyzer (EN2, ecom GmbH, Germany) and Fourier-transform infrared spectrophotometry (FTIR-7600, Lambda Scientific, Australia) and gas chromatography (Bruker 450-GC, USA) were employed to determine the NO_x, CO₂, OHC, and HC concentrations, respectively.

2.2.4. Properties of gliding arc plasma discharge

The high voltage was delivered in two modes: in load mode, the voltage was supplied to the reactor to generate the gliding arc plasma, whereas in non-load mode the high-voltage source was not connected with the plasma reactor. As presented in Figure 2.7(a), the high-voltage supply is sinusoidal during non-load operation. However, the voltage waveforms change significantly during GA plasma generation, i.e., the sinusoidal voltage waveform is transformed into pulsed waveforms and has numerous filaments (spikes) instead of the smooth line resulting from the non-load high voltage. The current corresponding to the voltage generated by the GA plasma is shown in Figure 2.7(b), which indicates high-intensity microstreamers [Figure 2.7(c)] that reach ampere levels and are superior to the current in a DBD[58] or honeycomb catalyst plasma discharge,[48] where the current intensities reach milli-ampere levels. The high current intensity of the GA plasma resulted from the low absolute impedance of the GA during plasma generation because of the small air gap without a dielectric layer between the two electrodes. Indeed, a DBD has a quartz tube as a dielectric layer,[58] whereas a honeycomb catalyst plasma reactor has a large electrode gap (52 mm) conjugated with the

honeycomb catalyst located inside the gap, which means that the impedance of the reactor is high.[47, 94] Because of the highly oscillating behavior of the electrical waveforms during GA plasma generation, the plasma discharge power was previously calculated by integrating the voltage and current data,[48] which does not produce a highly accurate result for the power. Consequently, in this study, the discharge power of the GA plasma was estimated on the basis of the power consumption, which was measured by a power meter and displayed on the control panel of the AC-based power supply.

Regarding the temperature of GA plasma, the gas temperature at the outlet of GA was monitored by a ceramic thermocouple; the tip of the ceramic thermocouple located at the center of the ground electrode tube of GA and distance from at the end of the power electrode was 30 mm. The surface temperature of the outer ground electrode of the GA was also measured. The evolution of gas temperature was recorded at an input power of 11 W, as shown in Figure 2.8. The temperature was increased sharply from room temperature to 68 °C within the initial 20 min and then gradually increased to the stable temperature at 73.4 °C; meanwhile, the outer surface temperature at a steady state was obtained at 84 °C. The low temperatures of gas and outer surface GA reactor can be explained by the reactor being exposed to ambient air and without covering thermal insulators. The gas outlet of GA was through a 60-cm stainless-steel pipe and then mixed with the remaining 10 L/min in the mixing chamber (3.5 L); the pipe and chamber were also exposed to ambient air. Consequently, the mixed gas temperature is close to room temperature, suggesting the gas temperature of GA did not affect the catalyst stage. Owing to a long movement time from the outlet GA to catalyst position (≥ 17.5 s), we supposed there are negligible effects of short/long life radicals forming during GA plasma on overall NO_x removal efficiency.

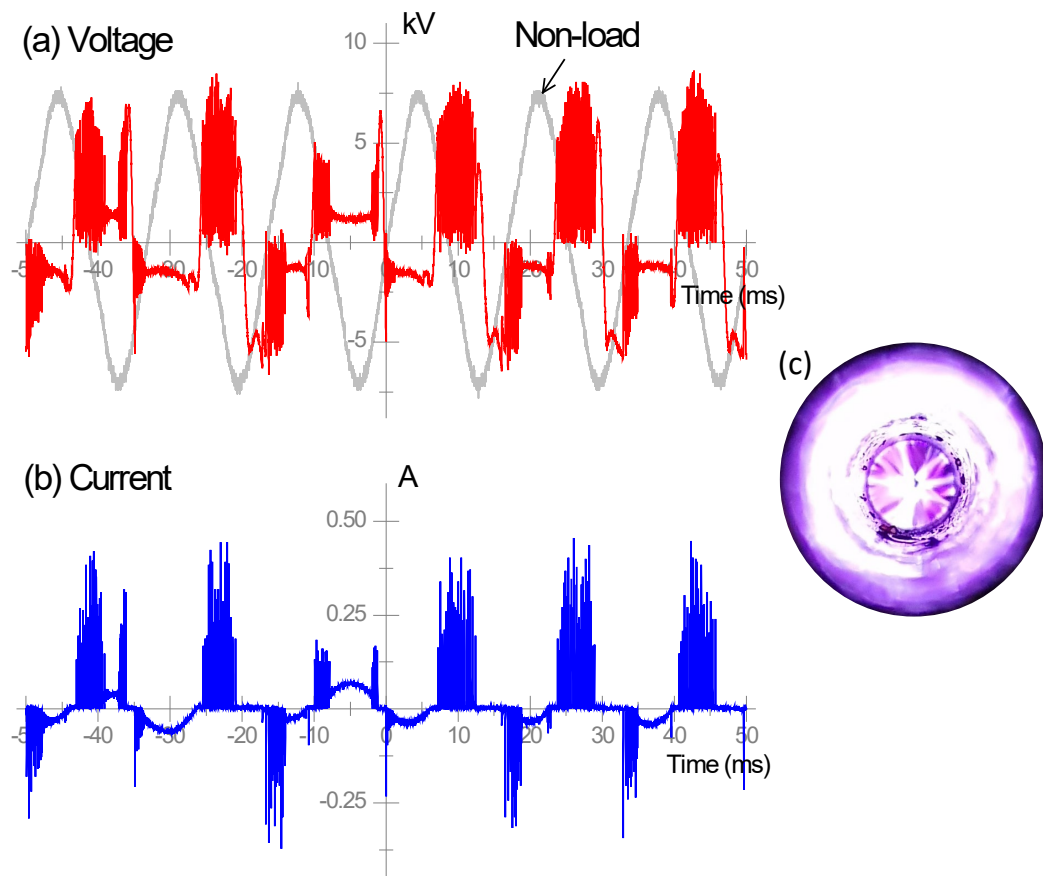


Figure 2.7. Electrical waveform of gliding arc plasma at input power of 11 W (a) voltage, (b) current, and (c) image of discharge (total flow rate of 2 L/min with $N_2/O_2 = 9/1$; $n\text{-heptane}_{inlet} = 2314 \text{ ppm}$).

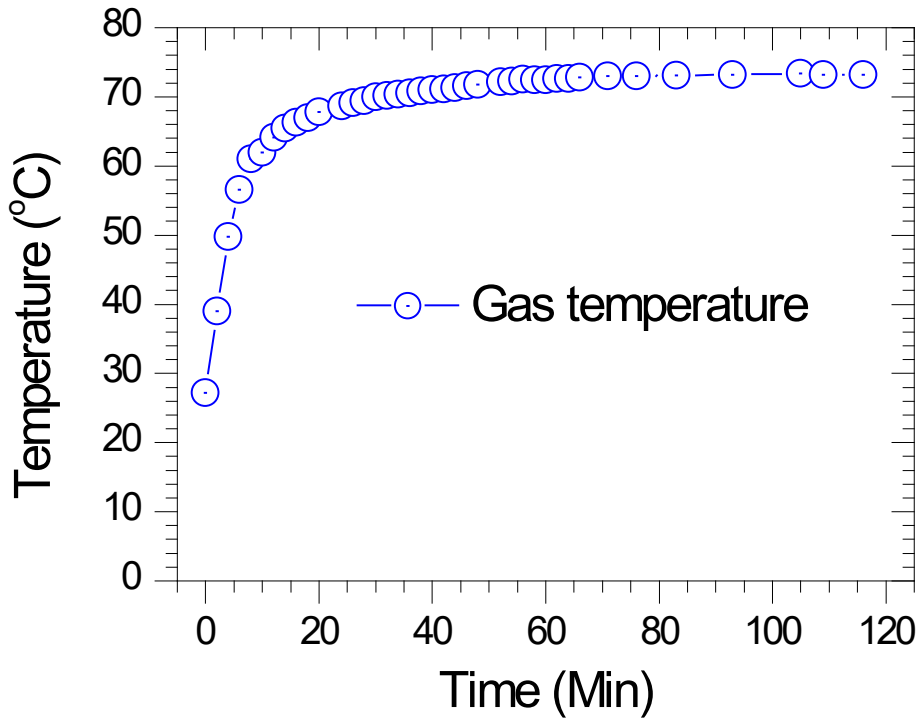


Figure 2.8. Gas temperature at the outlet of gliding arc plasma (input power = 11 W, total flow rate of 2 L/min with $N_2/O_2 = 9/1$; *n*-heptane inlet = 2314 ppm).

2.2.5. Term definition used for analyzing the result

The overall removal efficiency of NO_x was calculated using Eq. 2.2.5.1 after measuring the NO_x concentration of the feed gas and that at the gas outlet after the process. However, because additional NO_x is formed during exposure of the feed gas to the GA plasma, the absolute amount of NO_x passed to the catalyst stage increased. Consequently, the NO_x removal efficiency in the catalyst stage is obtained using Eq. 2.2.5.2, where the NO_x formation during the plasma stage is added. Other terms, such as the conversion of *n*-heptane, energy density in the plasma stage, and specific energy input (SEI) for the process, are defined in Eq. (2.2.5.3)-(2.2.5.5), respectively.

$$NO_x \text{ removal efficiency, } \eta(\%) = \left(1 - \frac{C_{NO_x}^{outlet}}{C_{NO_x}^{in feed}} \right) \times 100 \quad (2.2.5.1)$$

$$\eta(\%) \text{ for catalyst stage} = \left(\frac{C_{NO_x}^{in\ feed} + C_{NO_x}^{Arc} - C_{NO_x}^{outlet}}{C_{NO_x}^{in\ feed} + C_{NO_x}^{Arc}} \right) \times 100 \quad (2.2.5.2)$$

$$\text{Conversion of } n\text{-heptane}(\%) = \left(1 - \frac{C_{n\text{-heptane}}^{outlet}}{C_{n\text{-heptane}}^{in\ feed}} \right) \times 100 \quad (2.2.5.3)$$

$$\text{Energy density for plasma stage, ED} \left(\frac{J}{L} \right) = \frac{\text{Power consumption (W)}}{\text{Flow rate of plasma (L/min)}} \times 60 \quad (2.2.5.4)$$

$$\text{Specific energy input, SEI} \left(\frac{J}{L} \right) = \frac{\text{Power consumption (W)}}{\text{Total flow rate (L/min)}} \times 60 \quad (2.2.5.5)$$

The concentration of NO_x throughout the entire process was measured at the total flow rate of 12 L/min.

CHAPTER 3 – EFFECTIVE PRACTICAL REMOVAL OF ACETALDEHYDE BY A SANDWICH-TYPE PLASMA-IN-HONEYCOMB REACTOR UNDER SURROUNDING AMBIENT CONDITIONS

Chapter 3 is redrafted from:

Matyakubov Nosir et al. "Effective practical removal of acetaldehyde by a sandwich-type plasma-in-honeycomb reactor under surrounding ambient conditions." *Journal of Hazardous Materials* 415 (2021): 125608.

3.1. Introduction

This chapter focused on the removal of acetaldehyde in a honeycomb plasma reactor. Here, the plasma reactor was created by a commercial honeycomb catalyst located between two electrodes like a sandwich. The feed gas is a simulated indoor acetaldehyde emission, i.e., a low acetaldehyde concentration in a humidified air. The removal of acetaldehyde by the humidified air plasma was examined with several factors: concentration of acetaldehyde, humidity of feed gas, total flow rate, metal absence/presence on the monolith, input energy, and process time. As a result, the honeycomb plasma discharge is capable of acetaldehyde removal with extensive gas volume treatment at room temperature. Furthermore, the plasma chemistry of honeycomb discharge was also discussed in this study.

3.2. Experimental

The experimental setup, the configuration of corona plasma in honeycomb monolith, and analyzing methods of this work are discussed and presented in chapter two (2.1.1-2.1.3 sections).

3.3. Results and Discussion

3.3.1. Dependence of honeycomb discharge on acetaldehyde concentration and process time

The honeycomb discharge strongly depends on the physicochemical honeycomb surface, i.e., humidity, relative permittivity (dielectric constant), and conductivity [47, 48, 94]. In this

study, the effect of acetaldehyde on the plasma discharge was investigated under the presence or absence of 100 ppm acetaldehyde in the 70 L/min of humidified air (water content of 3.3 %). Herein, the high acetaldehyde inlet concentration was used to rapidly obtain a steady-state of acetaldehyde adsorption on the surface. The monolith catalyst was dried at 300 °C for 3 h to remove the contaminated chemicals and water; the monolith catalyst was cooled to 110 °C in the oven and then cooled back to room temperature inside a desiccator. The dried monolith catalyst was assembled into the reactor, and the humidified gas was fed through the reactor. The high voltage of 20 kV started power delivery to the electrodes; the discharge power and gas temperature were recorded during plasma discharge. The evolution of the discharge power and temperature with the absence/presence of acetaldehyde is shown in Figure 3.1.

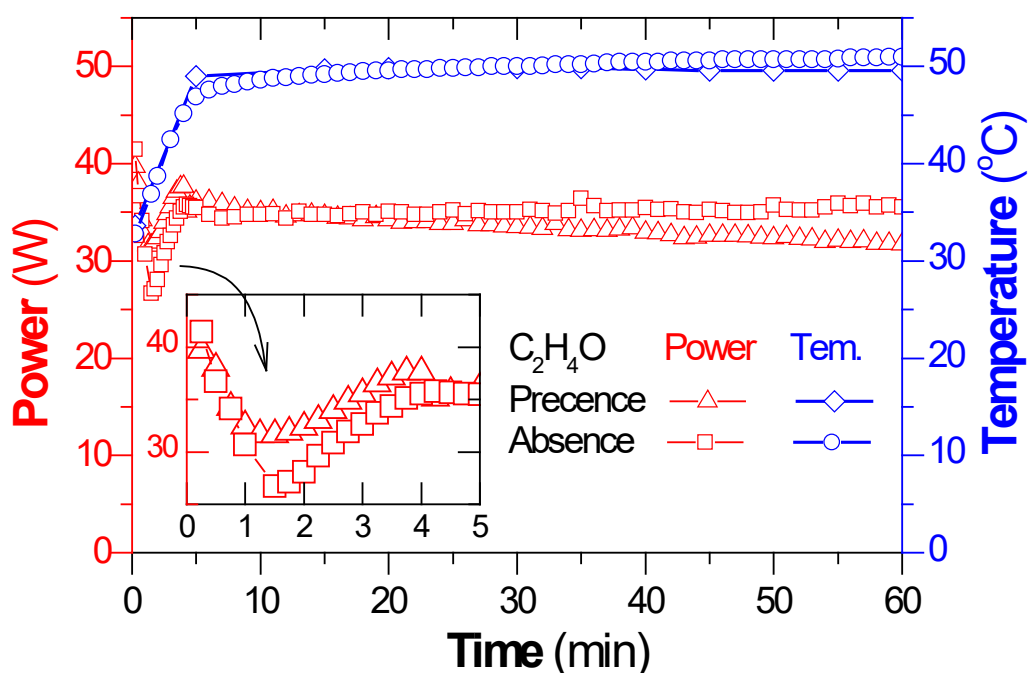


Figure 3.1. Effects of presence/absence of acetaldehyde on the discharge power and gas outlet temperature (Applied voltage = 20 kV; C_2H_4O inlet = 100 ppm; water content = 3.3%; total flow rate = 70 L/min).

This figure demonstrated a negligible effect of acetaldehyde on the gas temperature and early discharge power (< 20 min). However, for process time above 20 min, the discharge power decreased slightly in the acetaldehyde presence. Whereas, in the absence of acetaldehyde, the discharge power was maintained and reached the steady-state. Consequently, after 60 min, the discharge power with acetaldehyde equaled 89% of the discharge power without acetaldehyde, meaning that the discharge power decreased by 11%. The phenomenon can be explained by the change of physicochemical property of honeycomb channel surfaces after absorbing acetaldehyde from the feed gas. To sum up, although the concentration of acetaldehyde was at a level of 100 ppm, the discharge power of the honeycomb discharge still decreased with the presence of acetaldehyde in the feed gas. The acetaldehyde adsorption of the monoliths was given in Figure 3.2.

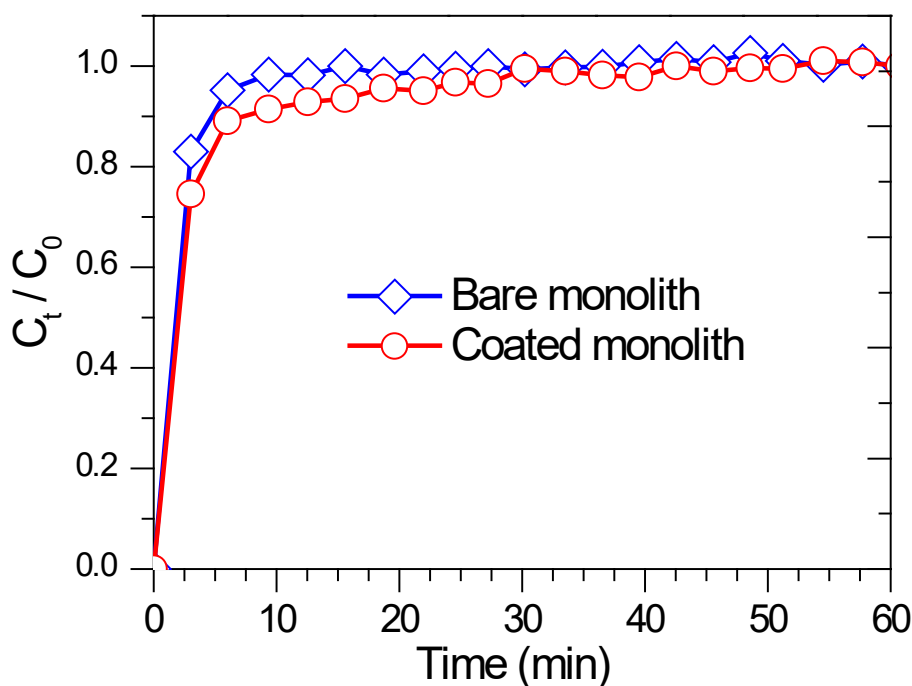


Figure 3.2. Comparison adsorbed acetaldehyde between the bare monolith and monolith catalyst under humidity of 2.5% (C_2H_4O inlet = 21 ppm; total flow rate = 40 L/min).

Effects of process time on the acetaldehyde removal were investigated in terms of SEI (discharge power) and acetaldehyde concentration in the gas outlet, as shown in Figure 3.3. The results revealed a low concentration of acetaldehyde in early time (20-min process time) in the gas outlet. After that, the concentration gradually increased and reached a steady-state at a processing time above 50 min. The adsorption of water and acetaldehyde by the monolith catalyst can explain both the low acetaldehyde concentration and humidity at the early time. As a result, the plasma process reached a steady-state after 50 min for all parameters; the conversion of acetaldehyde was about 39 % at these conditions. Consequently, in further experiments, all data were recorded when the process obtained a steady-state under these conditions. However, the outlet gas humidity rose rapidly within 5 min and reached the steady-state, as shown in Figure 3.4.

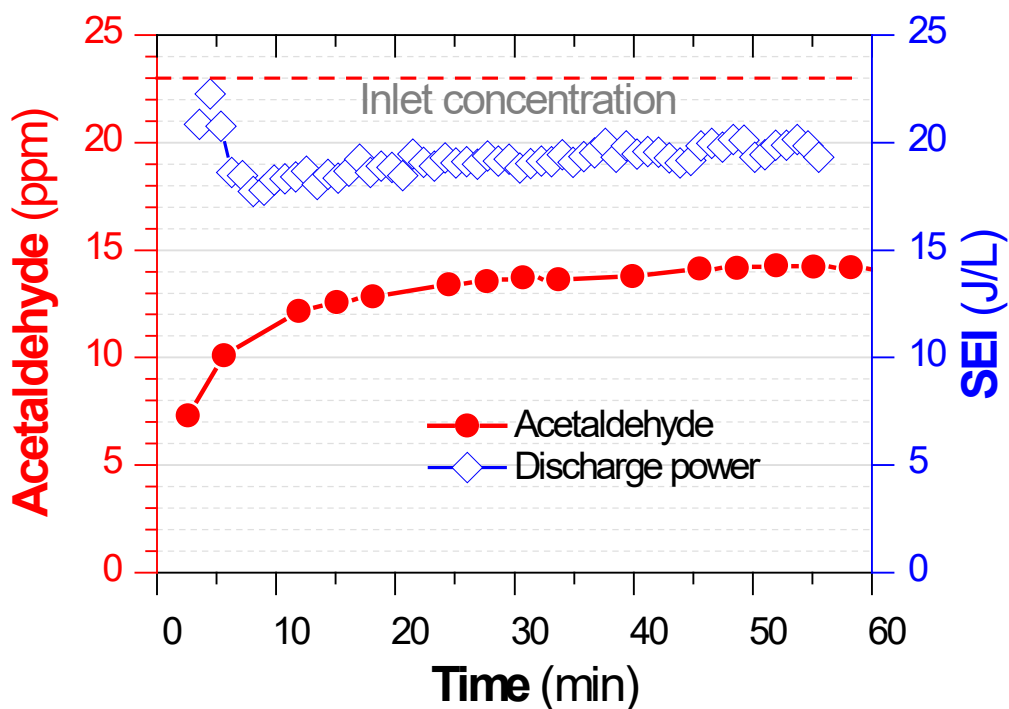


Figure 3.3. Evolution of the concentration of acetaldehyde and discharge power under applied voltage = 15 kV and water amount of 2.5% (C_2H_4O inlet = 23 ppm; total flow rate = 40 L/min).

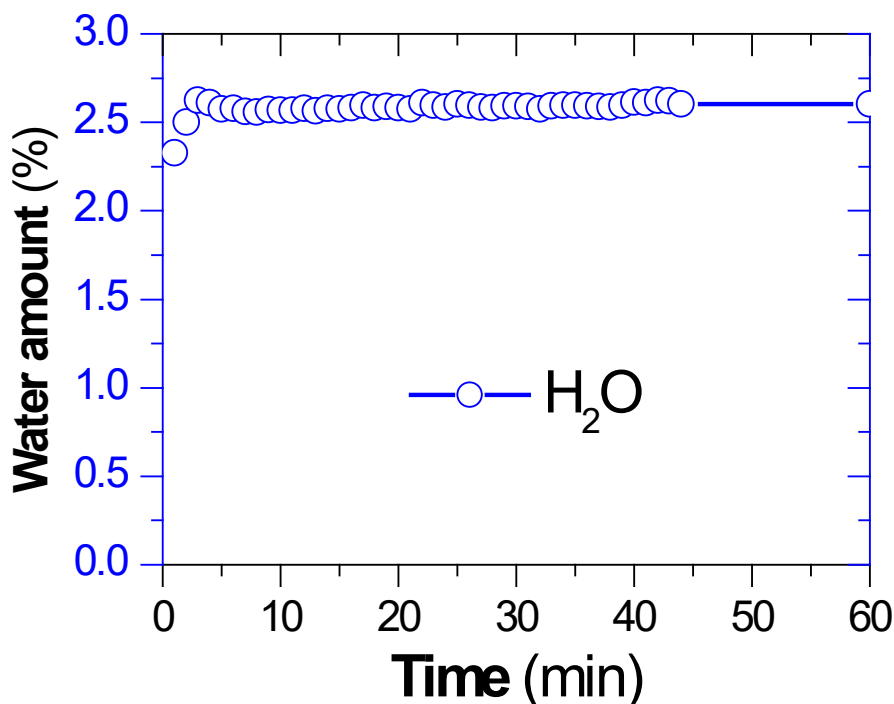
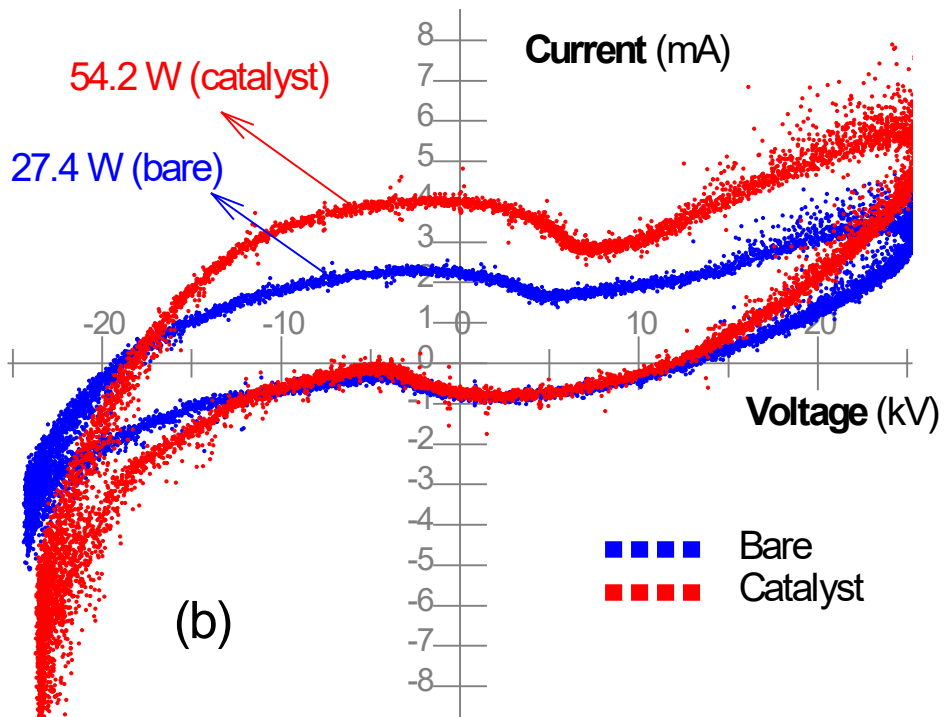
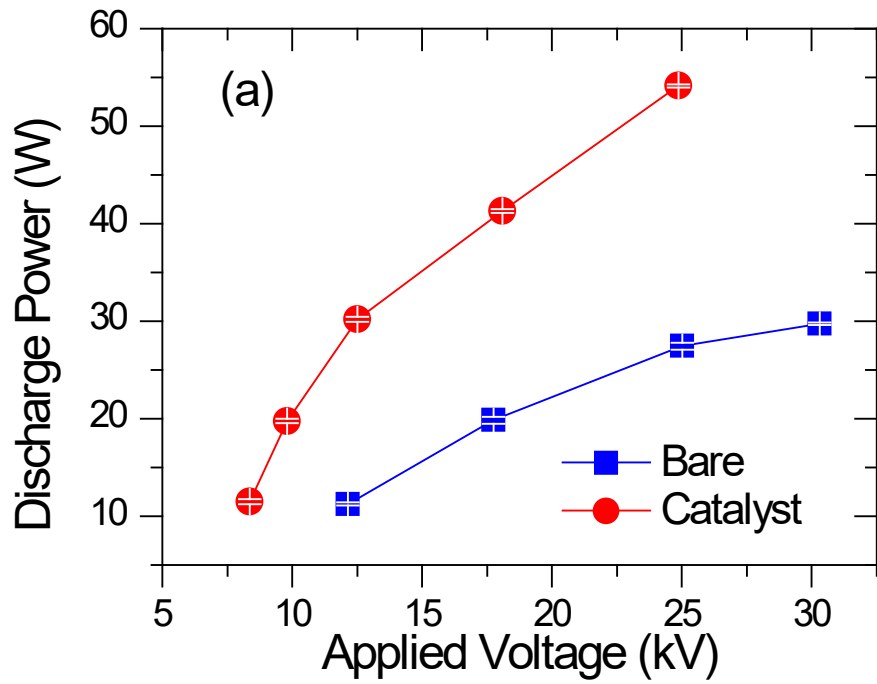


Figure 3.4. Evolution of the water amount during a honeycomb plasma discharge for removal of acetaldehyde (Applied voltage =15 kV; C₂H₄O inlet = 23ppm; total flow rate = 40 L/min).

3.3.2. A role of metal catalyst on the acetaldehyde removal process

Figure 3.5(a) showed the discharge power of the monolith catalyst was larger than that of the bare monolith under the same conditions. Precisely, at the same applied voltage, dissipated input energy on the monolith catalyst is superior to the bare monolith under the same other conditions. A high discharge power in the monolith catalyst resulted from the high intensity of the discharge current. Indeed, the discharge power is estimated by integrating instantaneous power (multiplication of voltage with the current), as given in Eq. (1). Therefore, under the same voltage, high intensities of current lead to high discharge power. For instance, the curves of voltage and discharge current under bare/catalytic monoliths are presented in Figure 3.5(b). This showed that the current intensities of catalyst are superior to bare, especially during plasma discharges (around high voltage peaks).



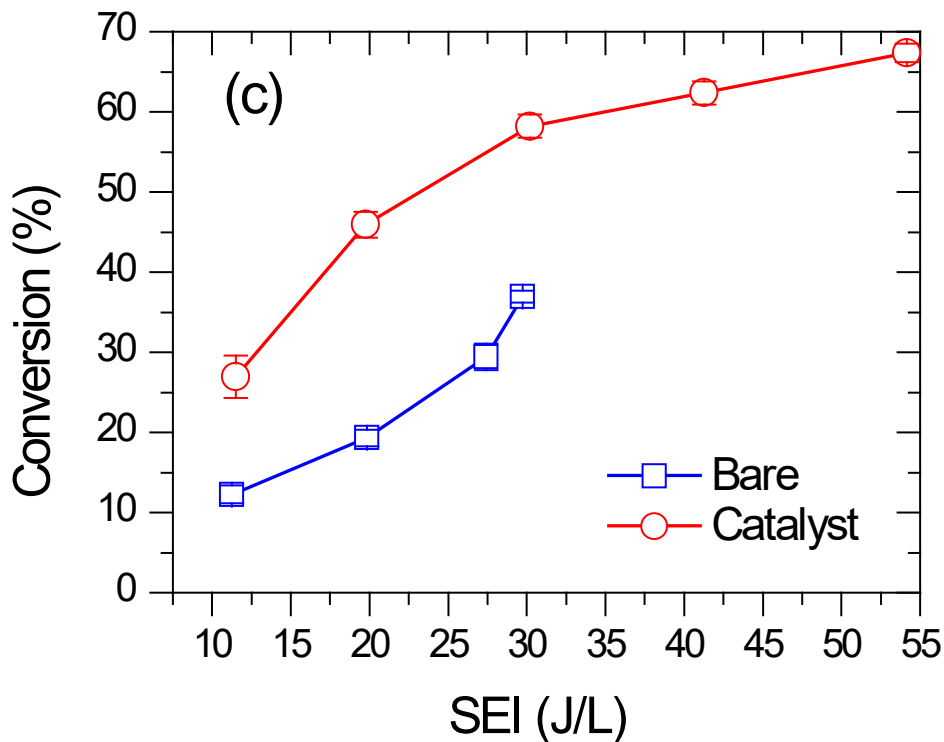


Figure 3.5. Comparison between the bare monolith and monolith catalyst on the (a) discharge power, (b) curve of voltage and current discharge at 25 kV, and (c) conversion of acetaldehyde (total flow rate = 60 L/min; water content = 2.5%; C₂H₄O inlet = 5 ppm).

As a result, the discharge power of the bare monolith is 27.4 W, while it is 54.2 W for the monolith catalyst case. The applied voltage required to obtain the same SEI is higher for the bare monolith than the monolith catalyst. The difference between the bare and catalytic monoliths on the discharge power can be explained by implementing the physicochemical surface of honeycomb channels due to the coated layer. Indeed, a total metal component of 0.23%, M/Al₂O₃ (M= Co, La, Pd, Pt), was present on the coated layer of monolith catalyst, whereas the bare monolith was made from 2MgO.2Al₂O₃.5SiO₂ (typical ceramic materials). Furthermore, the reactor's capacitance with the monolith catalyst was observed to be higher than that of the bare monolith; the capacitance also strongly depends on the humidified feed gas [47, 48]. The plasma discharge behavior in the sandwich-type honeycomb discharge

consisted of two stages in each phase of voltage (positive and negative), i.e., the capacitive stage and followed the discharge stage. Consequently, a larger capacitance leads to an increase in discharge current as well as discharge power [47, 48]. Furthermore, metals distributed on the surface of honeycomb channels would improve the electrical conductivity of the monolith; it is also a reason for increased discharge power with the monolith catalyst.

The effect of the coated layer on the conversion of acetaldehyde was also examined and presented in Figure 3.5(c). This indicated that the conversion via the catalyst is superior to bare at the same SEIs; moreover, the conversion rate increased towards SEI for both monolith cases. The different conversion of acetaldehyde under bare monolith/monolith catalyst is described by the coated layer presence on the monolith. This suggested that there is an incorporated effect of the coated layer with plasma for the acetaldehyde conversion in the honeycomb plasma discharge. To sum up, the commercial honeycomb catalyst with the presence of a metal coated layer improved discharge power and increased the acetaldehyde conversion by the plasma-catalytic reaction. Due to an extensive range of SEI that can be carried out with the monolith catalyst, high removal efficiency of acetaldehyde can be obtained by a plasma-catalyst discharge. For instance, about 67% of acetaldehyde in the gas inlet was converted at SEI of 54 J/L in the case of plasma-catalyst.

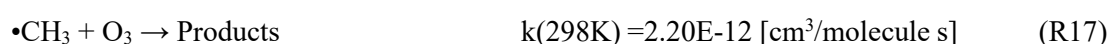
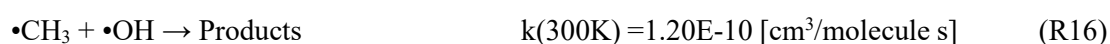
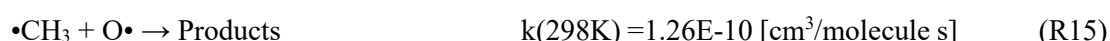
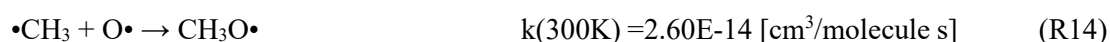
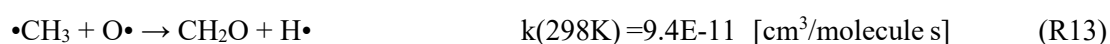
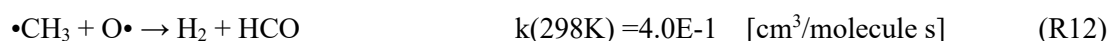
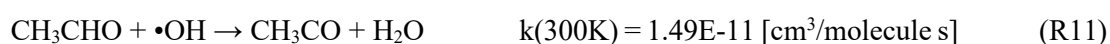
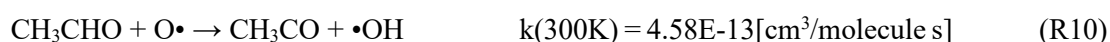
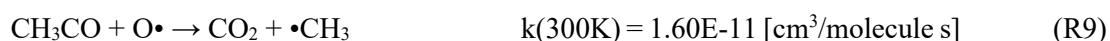
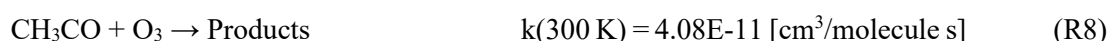
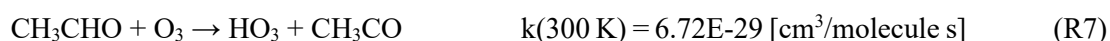
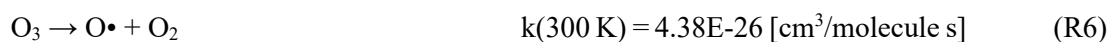
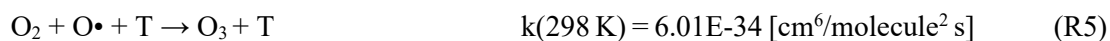
More activated sites in the honeycomb catalyst can explain the increased conversion rate of acetaldehyde with the honeycomb catalyst. Indeed, the conversion of acetaldehyde can occur in both gas phase and channel surfaces. Several possible reactions for acetaldehyde removal during plasma-catalyst discharge are given in R1-20; for referencing, their rate constants under the absence of plasma discharge at room temperature (300 K) were acquired from [95]. Herein, the reactions are interactions between $O\cdot$, $\cdot OH$, $\cdot CH_3$, $\cdot CHO$, and CH_3CHO molecules, due to low dissociation energy of O_2 , H_2O , and CH_3CHO (~ 5 eV); the phenomenon was supported by a negligible NO_x concentration in the gas outlet with/out acetaldehyde in the

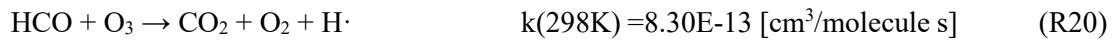
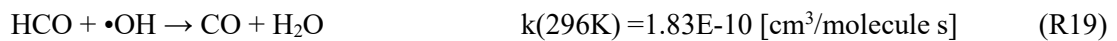
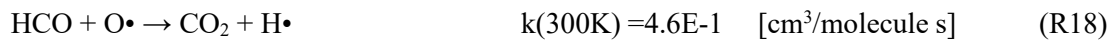
feed gas, due to considerable dissociation energy of N₂ (~9.79 eV). Since the coated catalyst layer improved the adsorption of reactive species and created more catalyst active sites, reactive species can be absorbed, followed by the reaction on those sites [36]. As a result, besides acetaldehyde converted by plasma reaction in the gas phase, the plasma-catalyst active sites have added the conversion.

Dissociation of gas molecules by e/M (excited species)



Possible main reactions between species for O₃ generation or acetaldehyde removal





3.3.3. Dependence of the acetaldehyde removal on the input parameters

3.3.3.1. Effects of flow rate on acetaldehyde removal process

Figure 3.6(a) presented that the conversion rate of acetaldehyde increased with the total gas flow from 20 to 60 L/min, corresponding to gas hourly space velocity (GHSV) from 3,500 to 10,600 h⁻¹, at the same SEI of 25 J/L. Since the concentration of acetaldehyde was fixed at 5 ppm in the feed during varying total flow rates, the absolute amount of acetaldehyde conversion significantly

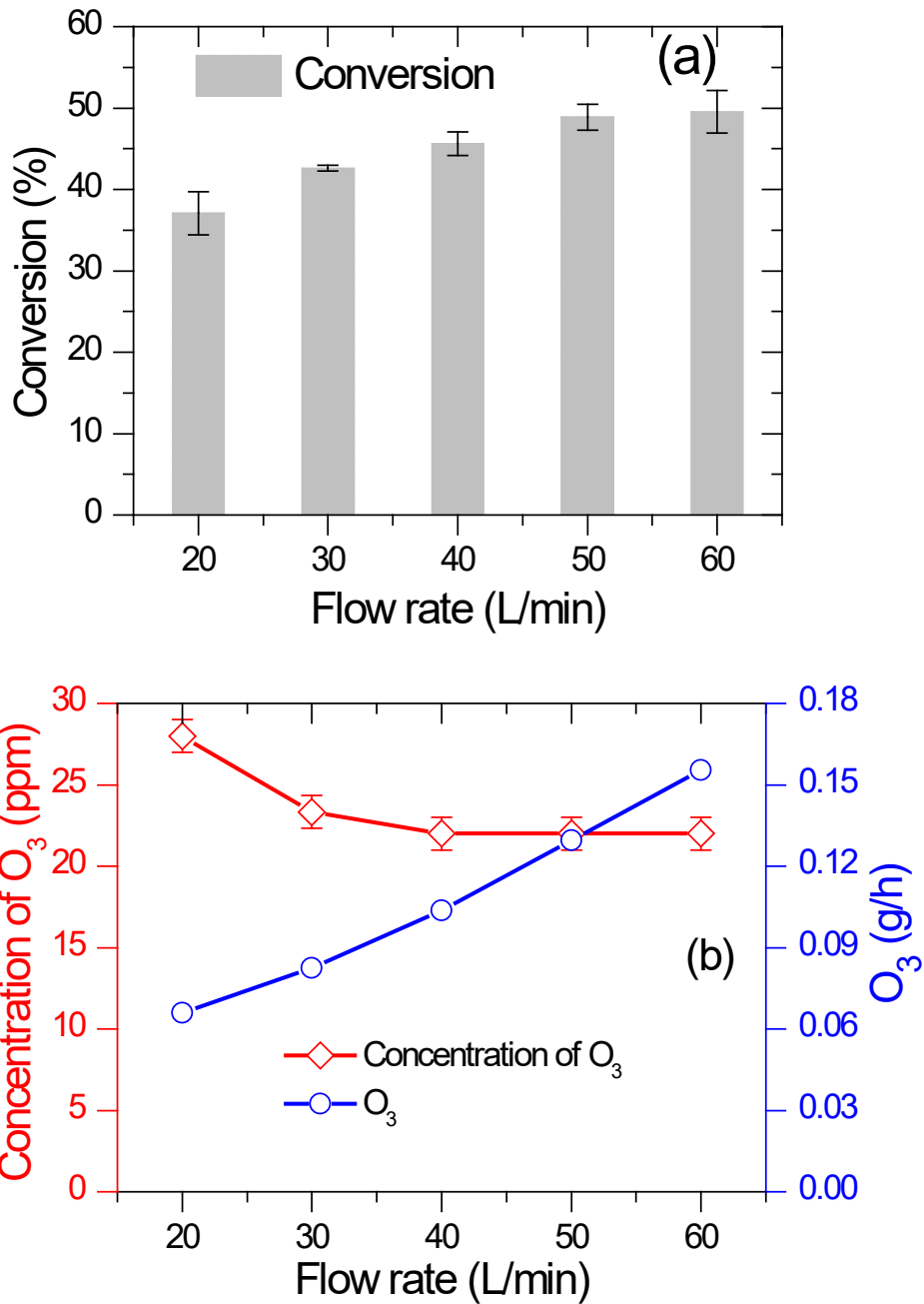


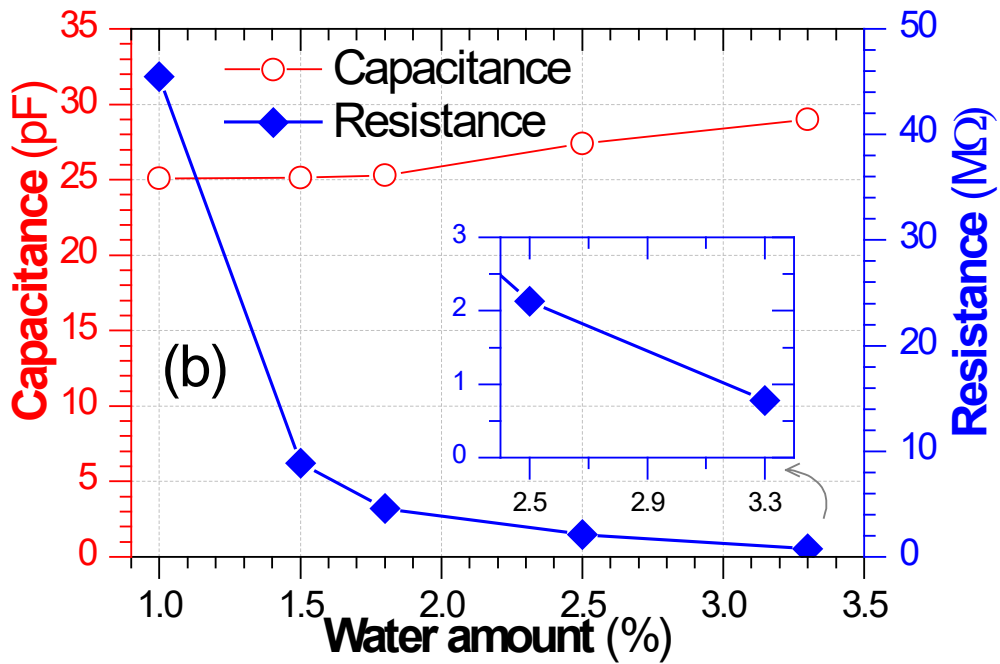
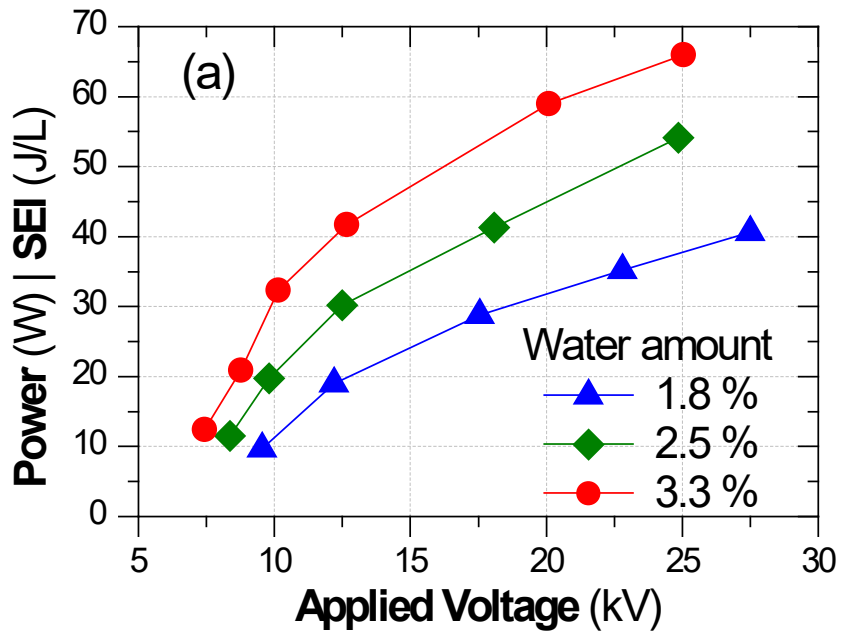
Figure 3.6. (a) effects of flow rate on the removal of acetaldehyde with inlet acetaldehyde fixed at 5 ppm and (b) formation of O₃ at SEI of 25 J/L under the absence of acetaldehyde (water content = 2.5 %).

increased toward the flow rate. Generally, when a decrease in the retention time by adjusting the flow rate, the conversion rate would be decreased [96]. However, in this study, the

phenomena did not occur with the retention time decreased from 0.48 to 0.16 s for a total flow rate of 20 and 60 L/min, respectively. A reason for explaining the result is a linear amount of $O\bullet/O_3$ generation with a total flow rate by the plasma system. To validate, the concentration and total amount of O_3 under the same conditions without acetaldehyde in the feed were plotted in Figure 3.6(b). The figure demonstrated that the experimental data are in agreement with the supposition. Specifically, the total O_3 generation increased from 0.07 to 0.16 g- O_3 /h toward the flow rate, although the concentration of O_3 decreased slightly from 28 to 22 ppm under this condition. Furthermore, the O_3 concentration in the gas outlet with 5-ppm acetaldehyde in the feed gas is 13 and 14 ppm with a total flow rate of 20 and 30 L/min, respectively. The significant O_3 emission, while incomplete acetaldehyde decomposition in the gas outlet, can be explained by massive O_2 (~205,000 ppm) in comparison to acetaldehyde (5-20 ppm) in the gas phase conjugated with the reaction rate of R5, which is comparable to other reactions with acetaldehyde as reactants (R7-20). To sum up, the conversion rate of acetaldehyde increased with the total flow rate.

3.3.3.2. Effects of the humidity on acetaldehyde removal process

Humidity has an adverse effect on the plasma for VOCs as well as acetaldehyde removal [97], owing to decreasing efficiency removal of VOC. Unfortunately, an indoor emission of VOC is a typical atmosphere that consisted of 1.5 to 3.5 % water vapor, which depends on the surrounding ambient conditions. However, the humidified feed gas is a critical factor for the plasma performance in the honeycomb discharge, i.e., poor honeycomb plasma discharge is solved with sufficient water vapor in the feed gas. In this study, the effect of water amount in the feed gas on the plasma performance for acetaldehyde removal was examined under varying SEI from 10 to 70 J/L.



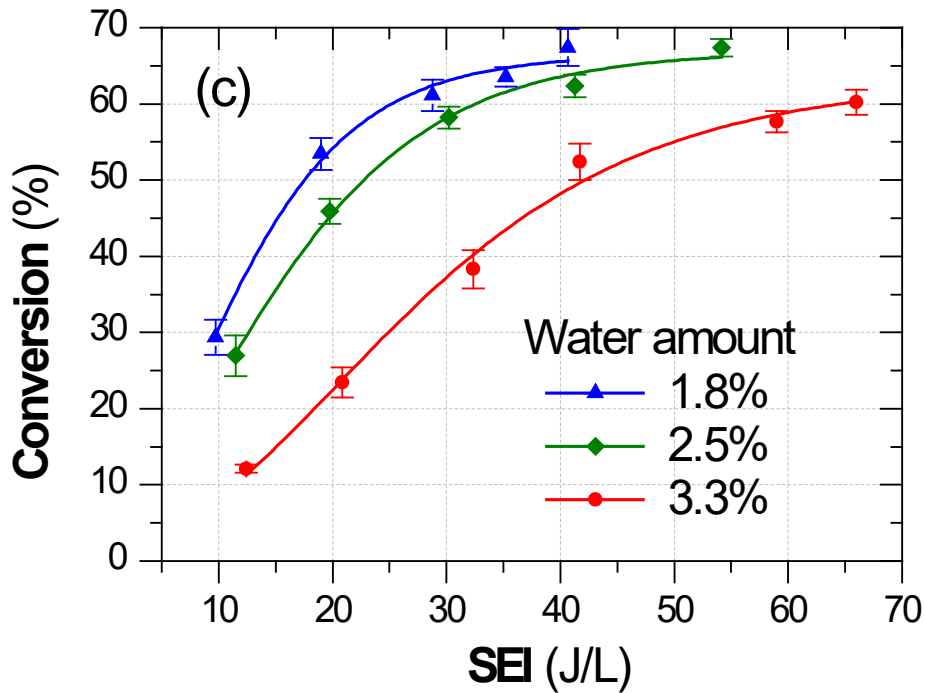


Figure 3.7. Effects of water amount in the feed gas on the (a) discharge power, (b) capacitor and resistance under without plasma discharge (the reactor was unconnected with plasma power supply), and (c) removal of acetaldehyde (C_2H_4O inlet = 5 ppm; total flow rate = 60 L/min).

Figure 3.7(a) demonstrated that the discharge power, as well as SEI, increased when the water amount in the feed increased at the same applied voltage. In other words, to obtain similar discharge power or SEI, the applied voltage requirement decreased at high humidity. The tendency is in agreement with that obtained by a bare monolith [48]. The increased discharge power can be explained by the significant decrease in resistance or increase of capacitance of the reactor under the high-water amount in the feed gas, as shown in Figure 3.7(b). As seen from this figure, the massive resistance (45.5 M Ω) at 1.0% water was suddenly dropped to a level of 9 M Ω when the water amount reached 1.5%. Consequently, the current intensity increased significantly, although the applied voltage was the same. As discharge

power is an integration of voltage and current, as shown in Eq. 1, a high discharge power was obtained under a high-water amount. In another viewpoint, the plasma discharge in a sandwich-type honeycomb plasma discharge is like DBD discharge, which consisted of charge and discharge phase [47, 48]; therefore, an increase in the reactor capacitance is a result for high plasma discharge. Both trends of the resistance and capacitance under the water variation in the feed gas agreed to increased plasma discharge.

In contrast, acetaldehyde conversion decreased towards increased water amount in the feed gas, as presented in Figure 3.7(c). This means that energy efficiency for acetaldehyde removal decreased at a high-water amount. A decrease in O_3 generation at a high humidified air plasma can explain the decrease in acetaldehyde conversion at a higher water amount in the feed [48]. Another reason could be the increased input power used to dissociate water and oxygen species ($O\cdot$, O_3) reacted with water or hydroxyl radicals ($\cdot OH$) under a larger water amount that resulted in a low acetaldehyde conversion. To sum up, humidity is an inhibitor of the acetaldehyde conversion in the honeycomb discharge, around 60% acetaldehyde (inlet 5 ppm) in the humidified air ($\leq 3.3\%$) can be converted under SEI of 60 J/L.

3.3.3.3. Effects of the initial acetaldehyde concentration on acetaldehyde removal process

The conversion rate of acetaldehyde decreased negligibly with the variation of inlet acetaldehyde concentration in the range of 5-20 ppm, as presented in Figure 3.8. In detail, under the variation of inlet concentration, the conversion rate slightly decreased from 67.4 to 65.7% at SEI of 55 J/L and water content of 2.5%. Suggesting the removal efficiency of acetaldehyde is maintained by the system despite the changes in the inlet concentration. In other words, more acetaldehyde molecules can be destroyed by the plasma-catalyst discharge under these conditions. The emission of O_3 during this experiment was also plotted; this indicated the O_3 was emitted at the level of 25-30 ppm.

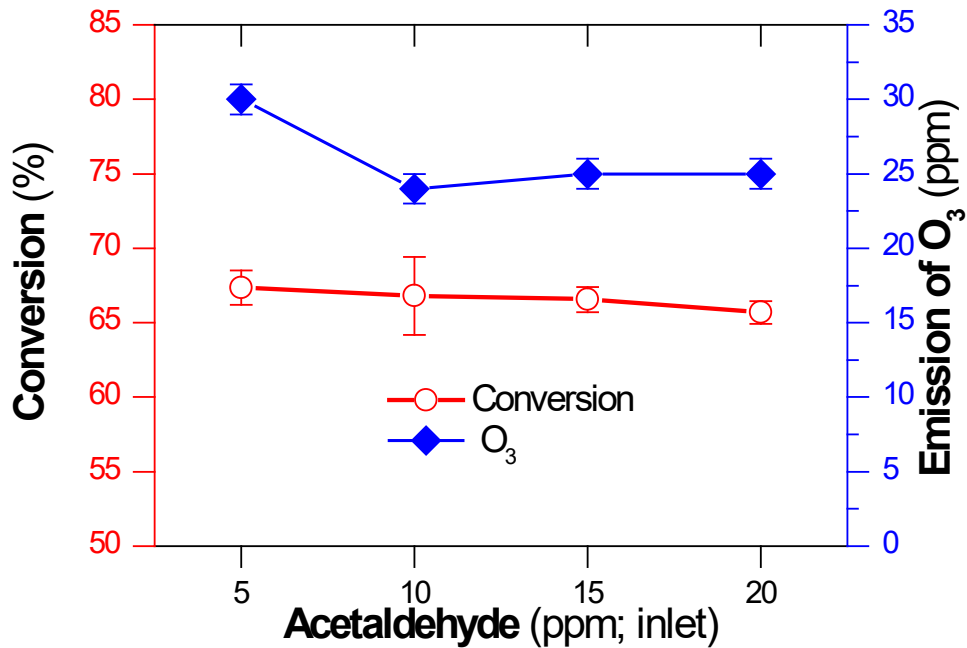


Figure 3.8. Effects of initial concentration of acetaldehyde on the conversion rate (total flow rate = 60 L/min; water amount = 2.5%; SEI = 55 J/L).

3.3.4. Plasma chemistry of honeycomb discharge

OES of the honeycomb plasma discharge from the 2-mm gap, the power electrode and honeycomb monolith catalyst, is shown in Figure 3.9. The typical spectrum is similar to other humidified air plasma spectra [94], which consisted of high intensities of N₂ line in C³Π_u – B³Π_g system (the second positive system of N₂) and N₂⁺ lines with B²Σ_u⁺ – X²Σ_g⁺ system (the first negative system of N₂⁺) [98]. Moreover, the NO lines from 200 to 300 nm in the A²Σ⁺ → X²Π system (nitrogen third positive, γ system) were also not detected (inset figure). Due to water presence in the discharge zone, there is a potential presence of OH lines in the spectra. However, with the high-intensity emission of N₂ background gas, the OH lines have been observed unclearly in the spectrum. Specifically, the OH lines at 295 and 308 nm can be merged with the N₂ emission at 296 and 315 nm, respectively. In the case of the 390 nm OH line, the line can be identified due to incomplete merger with 394 nm N₂ line, as presented in

the inset figure; as seen from this figure, the C_2 band at 516 nm was also not observed, although 5 ppm acetaldehyde was in the feed. The O_3 concentration was detected at 30 ppm in the gas outlet; however, the O lines at 777 nm and 884 nm were also not identified in the spectrum [99]. Consequently, under the humid condition and atmospheric, the OES of the honeycomb discharge is primary emissions of N_2 and N_2^+ in the range of [290-460 nm].

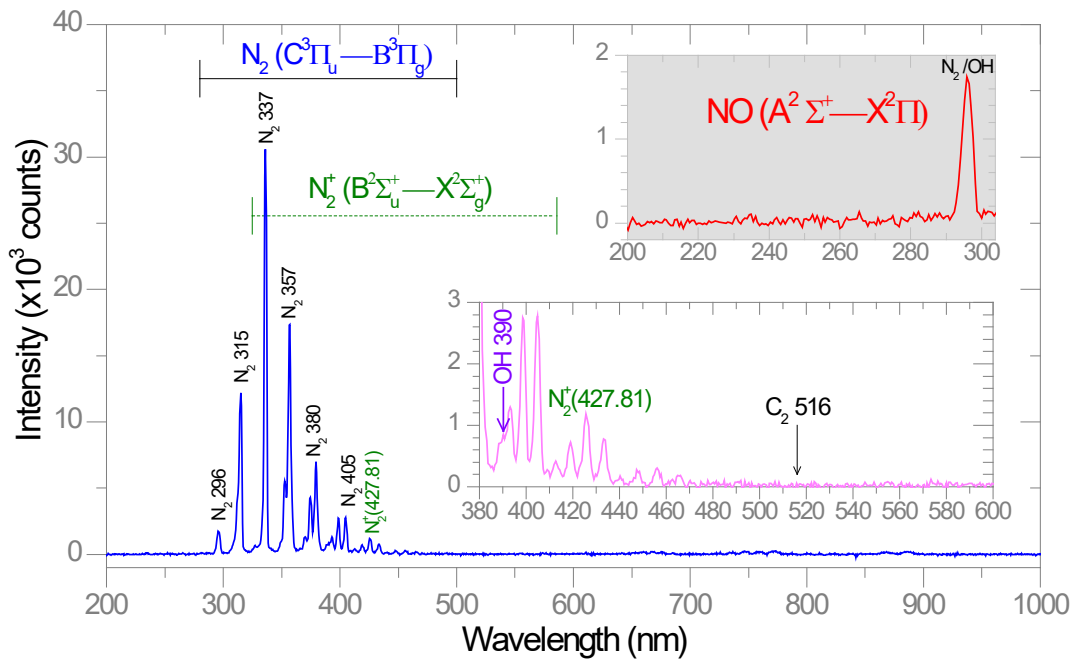


Figure 3.9. Optical emission spectrum at 2-mm discharge gap of high-voltage electrode and monolith catalyst at SEI of 40 J/L (total flow rate = 60 L/min; water amount = 2.5%; SEI = 40 J/L; C_2H_4O inlet = 5 ppm).

3.3.5. Comparison of acetaldehyde removal by the honeycomb plasma with other processes

A comparison between thermal reactivated catalyst and plasma-catalyst for acetaldehyde removal in humid air was shown in Figure 3.10. The figure demonstrated that the energy consumption of plasma-catalyst was supper less than that of thermal reactivated catalyst. Specifically, the gap between the two methods is approximately 200 J/L for obtaining the same acetaldehyde conversion in the range of 25-70 %. The significant difference between the two

methods can be explained by a NTP, which features electrons, ions, radicals, excited species (a chemical cocktail of reactive species, as presented in the OES), despite low temperatures of gas molecules. Fortunately, the interaction between the humidified air plasma and the surface of the monolith catalyst improved acetaldehyde removal at low temperatures instead of high temperatures in the thermal process. The required high temperature of the thermal reactivated catalyst is a disadvantage because the contaminated gas is close to room temperature; therefore, equivalent SEI is above 200 J/L to reactivate catalyst by heating the gas inlet and catalyst. In contrast with the plasma reactivated catalyst, it only consumed several tens of J/L to produce the chemical cocktails and converted acetaldehyde. In summary, the plasma-activated catalyst for acetaldehyde removal is superior to the thermal catalytic process. However, the limited input power dissipated on the honeycomb monolith need to be overcome for completing the removal of acetaldehyde by the plasma-catalyst.

A comparison between several plasma-catalyst systems for acetaldehyde removal is presented in Table 3. This indicated that almost all processes by either one stage or two stages of plasma with catalyst require energy consumption at a level of 100 J/L for acetaldehyde removal, which also validated again for the low-energy consumption by NTPs, as mentioned above. In comparison between the sandwich-type honeycomb plasma discharge and other plasma-catalyst processes, the energy efficiency by the honeycomb discharge is the lowest. The lowest energy efficiency can be explained by the lowest inlet concentration of acetaldehyde (5 ppm). It should be mentioned that high-energy consumptions would be required to treat a few ppm contaminated chemicals in background gases [100, 101]. Another reason is that high humidities in the feed gas led to a decrease in energy efficiency (section 3.3). However, in the feed gas case, the honeycomb discharge operated under high throughput and humid conditions. In summary, the acetaldehyde removal by the honeycomb plasma discharge showed a comparable removal efficiency with other processes. The system operated

with the simulated indoor emission of acetaldehyde as the feed gas, suggesting its practical applicability for acetaldehyde removal.

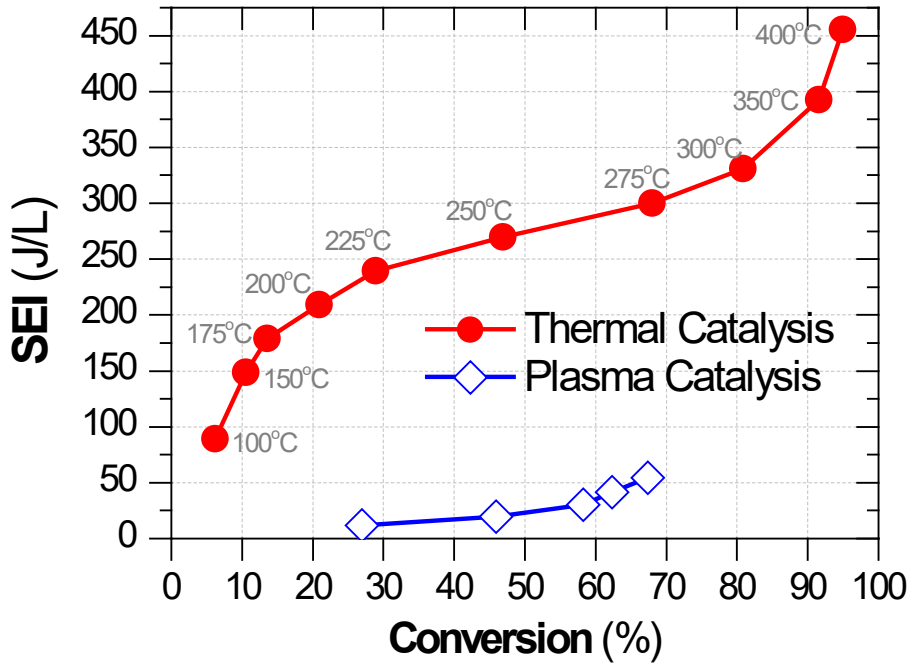


Figure 3.10. A Comparison between thermal catalytic activity and plasma for acetaldehyde conversion based SEI consumption (GHSV = 10,600 h⁻¹; water amount = 2.5%; C₂H₄O inlet = 5 ppm).

Table 3.1. A comparison between several plasma-catalyst systems for acetaldehyde removal process under atmospheric pressure conditions.

Type of reactor		Catalyst		Flow rate	H ₂ O	GHSV [□]	C ₂ H ₄ O (inlet)	SEI	η	EE	Ref.
Plasma	Configuration	Materials	Shape	L/min	%	h ⁻¹	ppm	J/L	%	(g/kWh)	
Corona	Plasma alone	-	-	N/A	0	N/A	500	210	95	14.7	[20]
	Plasma alone	-	-	1	0	1340	200	380	77	2.63	[96]
DBD	Two stages	Mn-Co/HZSM-5	Powder	1	0	1340	200	380	~96	3.3	
DBD	Plasma alone	-	-	0.1	0	1270	500	300	70	7.6	[102]
	One stage	Au/TiO ₂ /SiO ₂	Bead	0.1	0	1270	500	150	97	42.60	
DBD	Plasma alone	-	-	0.1	0	1270	500	150	25	5.4	[103]
	One stage	Ag/TiO ₂ /SiO ₂	Pellet	0.1	0	1270	500	150	97	21	
DBD	Plasma alone	-	-	0.1	0	1270	500	150	55	11.9	[101]
	One stage	Ag/TiO ₂ /SiO ₂	Pellet	0.1	0	1270	500	70/350/1150	33/87/98	15.3/8.1/2.8	
SHD	One stage	M/Al ₂ O ₃ (M= Co, La, Pd, Pt)	Honeycomb	60	1.8/2.5/3.3	10192	5	40/54/66	67/67/60	0.54/0.40/0.30	This work

SHD: Sandwich-type honeycomb plasma discharge; SEI: specific energy input; η: removal efficiency; EE: energy efficiency; GHSV[□] was calculated based on the volume of plasma/-catalyst discharge zone.

3.4. Summary

A honeycomb plasma discharge in a sandwich-type honeycomb plasma reactor presented high performance of acetaldehyde removal in the simulated indoor emission of acetaldehyde. The result displayed that the presence of metal catalysts on the monolith surface is very important to obtain higher discharge power, resulting in elevated acetaldehyde conversion. Additionally, the increased flow rate positively affected acetaldehyde conversion due to the increased $O\bullet/O_3$ generation toward raised flow rate at constant SEI and acetaldehyde concentration. Moreover, the removal efficiency also strongly depended on the humidified air, i.e., the conversion rate of acetaldehyde decreased at higher humidification of air. However, the plasma-catalyst system featured at least 60% conversion of acetaldehyde in the contaminated gas under SEI of 60 J/L and atmospheric humidity from 1.8 to 3.3%. The honeycomb discharge performance of acetaldehyde removal is superior to the thermal catalyst process due to lesser energy consumption; it is also comparable with other plasma-catalyst systems.

CHAPTER 4 – ENHANCING THE SELECTIVE CATALYTIC REDUCTION OF NO_x AT LOW TEMPERATURE BY PRETREATMENT OF HYDROCARBONS IN A GLIDING ARC PLASMA

Chapter 4 is redrafted from:

Matyakubov Nosir et al. "Enhancing the Selective Catalytic Reduction of NO_x at Low Temperature by Pretreatment of Hydrocarbons in a Gliding Arc Plasma." *Industrial & Engineering Chemistry Research* (2022).

4.1. Introduction

Chapter 4 focused on the pretreatment of an injected HC flow by GA plasma and its effect on the HC-SCR of NO_x in the low-temperature range (150–350 °C). In particular, Ag/γ-Al₂O₃ pellets containing 2% silver were employed for selective catalytic reduction, while *n*-heptane was used as the hydrocarbon reducing agent because *n*-dodecane (typical diesel fuel simulant) has a too low vapor pressure at room temperature to be injected by vaporizing. Ag/γ-Al₂O₃ is a promising catalyst for the selective reduction of NO_x because it is composed of inexpensive materials. First, the catalyst for NO_x removal was evaluated with several OHCs and *n*-heptane, the ratio of C₁/N in the feed, and the effect of the amount of water. Afterward, the extent to which NO_x removal was enhanced by pretreatment of the HC flow by the GA plasma and the mechanism thereof was examined. The results revealed that the NO_x removal efficiency was increased significantly by pretreatment with GA plasma because the *n*-heptane in the feed was oxidized to OHCs by the plasma discharge. This was confirmed by the optical emission spectra of the GA plasma, which suggested the formation of radicals and excited species during the conversion of *n*-heptane to OHCs by the GA plasma.

4.2. Experimental

Experimental setup, catalyst preparation, properties of gliding arc plasma, and analyzing methods of this work are discussed and presented in chapter two (2.2.2-2.2.5 sections).

4.3. Results and Discussion

4.3.1. Performance of NO_x removal over Ag/γ-Al₂O₃ catalyst in the low-temperature range

This section presents the evaluation of the NO_x removal performance over the Ag/γ-Al₂O₃ catalyst in a low-temperature range from 165 to 330 °C. The evaluations were performed by assessing the dependence of the NO_x removal efficiency on the various reducing agents, using the ratio of C₁ per NO_x, and the water content of the feed gas.

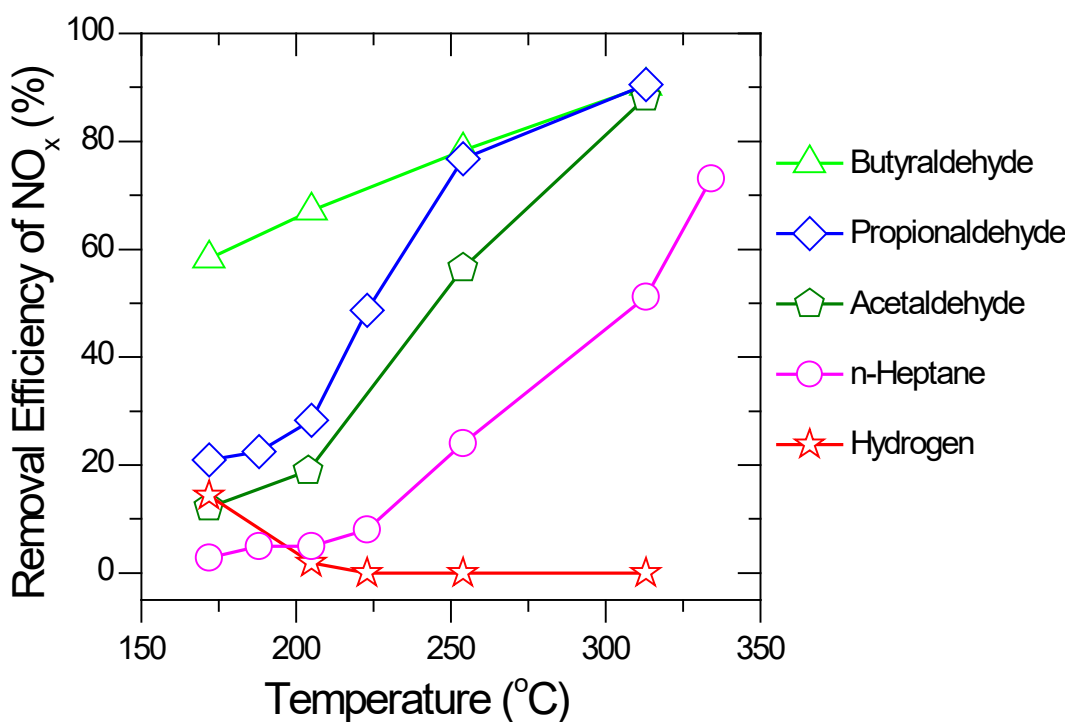


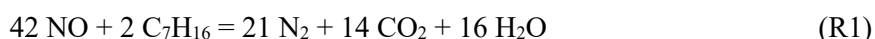
Figure 4.1. Dependence of NO_x conversion on reducing agent at different temperatures (GHSV=5000 h⁻¹; NO_{inlet}=300 ppm; C₁/N = 6; water content = 1.7 %; total flow rate = 12 L/min).

4.3.1.1. Dependence of NO_x removal efficiency on the reducing agent

Figure 4.1 presents the removal efficiency of NO_x with OHCs (several aldehydes), *n*-heptane, and hydrogen. These results indicate that the removal efficiency of NO_x is significantly dependent on the particular chemical compound used as the reducing agent. Specifically, aldehyde derivatives were more effective than *n*-heptane (an alkane). Among the aldehydes examined, the removal efficiency depended on the length of the carbon chain, i.e., the efficiency increased in the order acetaldehyde < propionaldehyde < butyraldehyde. Three possible explanations could exist for this result. First, the lower vapor pressure of compounds with a longer carbon chain[104] enhances the adsorption of reducing agents on the surface of the catalyst. Second, more derivatives and radical hydrocarbons can be formed from a compound with a longer carbon chain, e.g., the dissociation energy of the C–C bond is known to decrease with a long carbon chain.[105] Third, the chemical activity of an aldehyde functional group attached to a longer alkyl chain is higher. The temperature dependence of the NO_x removal efficiency in the presence of aldehydes or *n*-heptane was the opposite to that of H₂. Specifically, the removal efficiency of NO_x increased with temperature for the oxygenated/- hydrocarbons, whereas it decreased in the case of H₂. This suggests that hydrogen is a promising reducing agent for NO_x at low temperature, at an effective catalyst temperature of approximately 100 °C.[106, 107]

4.3.1.2. Effect of the C₁/N ratio on the removal efficiency of NO_x

In the redox reaction between NO and C_nH_{2n+2} (alkane) to form N₂ and CO₂, the stoichiometric ratio of C₁/N is 1/3; for instance, the redox reaction between NO and *n*-heptane is given in (R1).



Unfortunately, to ensure high removal efficiency, the C₁/N ratio used in the HC-SCR of NO_x is always higher than the coefficient ratio.[108, 109] In this study, the dependence of the

removal efficiency on the C_1/N ratio was examined by varying the ratio from 4 to 20 at a catalyst operating temperature of 252 °C using *n*-heptane as the reducing agent; the result is shown in Figure 4.2. As seen in the figure, the removal efficiency increased sharply as the C_1/N ratio changed from 4 to 9, followed by a more gradual increase as the ratio further increased to 15. The removal efficiency subsequently stabilized at ratios from 15 to 20. The dependence of the removal efficiency of NO_x on the C_1/N ratio can be understood by considering that a higher ratio means an increased concentration of reducing agents, with more reducing agent in the feed gas enhancing the probability of interaction between NO and the reducing agents on the catalyst. Considering the removal efficiency with *n*-heptane consumption, we selected a C_1/N ratio equal to 9 for further experiments.

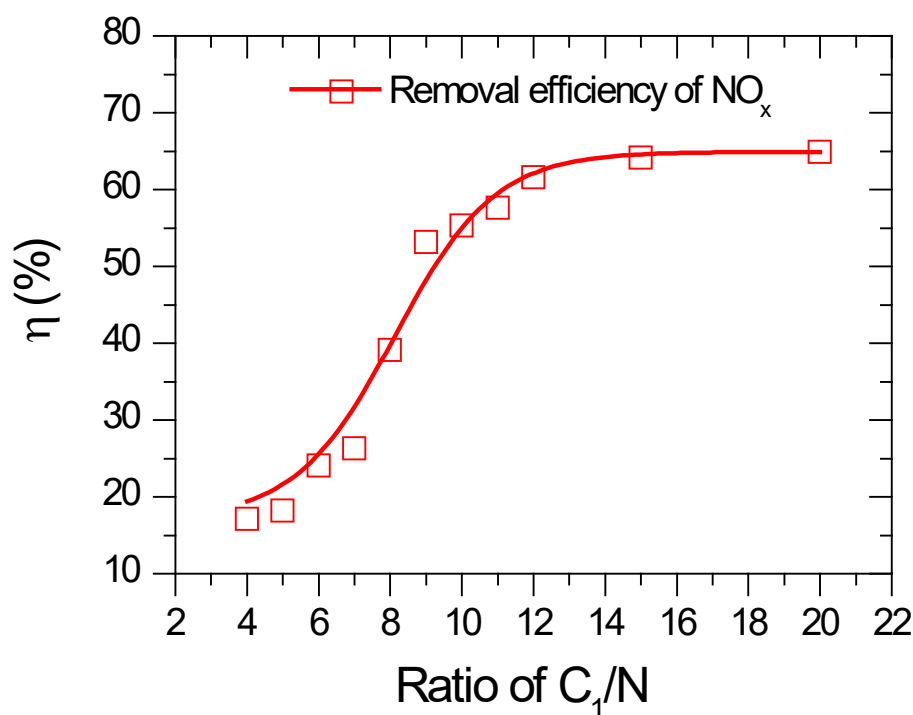


Figure 4.2. Effect of C_1/N ratio on the NO_x conversion under *n*-heptane as the reducing agent at 252°C (GHSV=5000 h^{-1} ; NO_{inlet} =300 ppm; water content = 1.7 %; total flow rate = 12 L/min).

4.3.1.3. Effect of water content on the removal efficiency of NO_x

Diesel exhaust gas, a product of the combustion of diesel fuel, has water as its main component ranging from 2% to 10%(v/v) [110]. This section presents our examination of the effect of the amount of water (from 1.7 to 3.5 %) on the removal efficiency of NO_x at 252 °C, as shown in Figure 4.3. These results indicate that the removal efficiency decreases with increasing the water content of the feed gas. This could be explained by considering the lower probability of interaction between NO_x and the reducing agent at activated catalyst sites, which would be occupied by the H₂O molecules in the feed gas with high concentrations of H₂O; indeed, the water concentration is at a level of ten thousand ppm, whereas the concentrations of the chemical reactants (NO_x, OHCs, HCs, and radicals) are much less. This result is in agreement with previous results where the presence of water was also found to negatively affect the NO_x removal efficiency [111, 112].

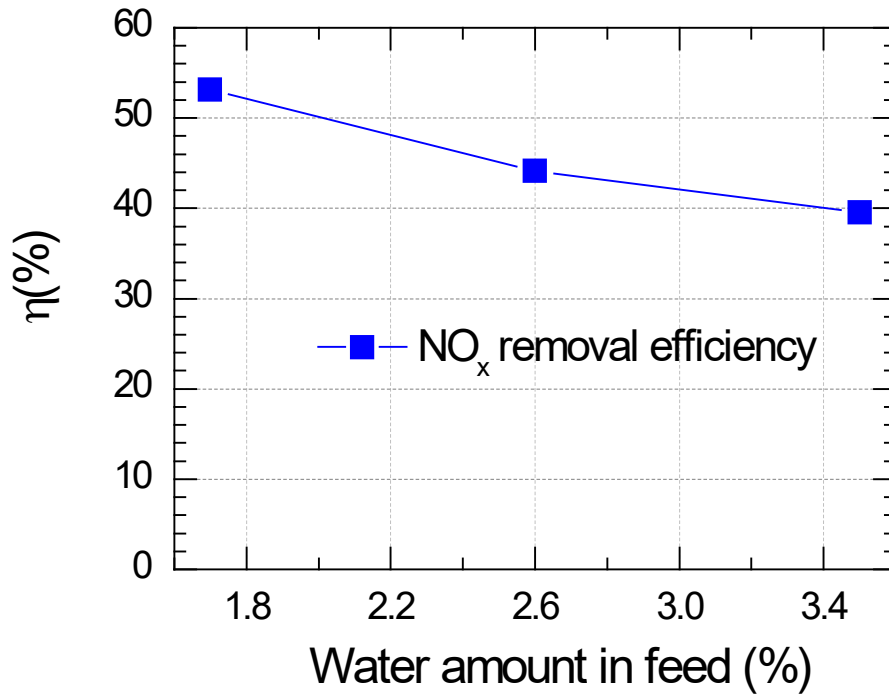


Figure 4.3. Effect of the water content of the feed gas on the removal efficiency of NO_x at 252 °C (total flow rate = 12 L/min; NO_{inlet}=300 ppm and *n*-heptane as reducing agent with C/N=9).

4.3.2. Improvement of NO_x removal by gliding arc plasma

4.3.2.1. Enhancing the removal efficiency of NO_x

The above results indicate that OHCs are more effective for NO_x removal than its parent HC. This suggests that a combination of the oxidation of the HC feed followed by injection into the main diesel exhaust gas stream would improve the NO_x removal efficiency of the catalyst in the low-temperature range. To validate this idea, *n*-heptane was oxidized by GA plasma to form OHCs and then injected into the main stream with a plasma flow rate fraction of 1/6. Finally, the mixture was passed through the catalyst at various temperatures; the NO_x removal efficiency under the same conditions but without plasma discharge was also recorded for comparison purposes. As a result, the NO_x removal efficiency significantly increased in

the low-temperature range with the pretreatment of the *n*-heptane gas stream by GA plasma, as shown in Figure 4.4. However, at temperatures above 250 °C, the use of plasma did not improve the removal efficiency and even lowered the removal efficiency because of the formation of NO_x and CO₂ in the GA plasma. The increase in the removal efficiency of NO_x resulted from the presence of OHCs in the feed gas as a result of the oxidation of *n*-heptane by the GA plasma. This finding was validated by analyzing the gas components by GC; meanwhile, the peaks were identified by comparing the retention time/shape of peaks in the chromatograms with those of standard samples using the same GC analysis method. Consequently, the chromatograms of both the feed gas (plasma off) and the gas at the outlet (plasma on) were recorded and are presented in Figure 4.5. These chromatograms demonstrate that the *n*-heptane in the feed was partly oxidized to form OHCs and other HCs, i.e., acetaldehyde, propionaldehyde, butyraldehyde, ethylene, and so on. In comparison with the efficiency of using plasma for the removal of NO_x that was previously reported,[56] where all the feed gas instead of part of the feed gas was pretreated with honeycomb catalyst plasma discharge, the removal efficiency of the plasma in this work was lower. The oxidation of NO to form NO₂ in the feed gas in addition to the formation of OHCs might explain this observation in the previous work; consequently, the catalyst stage is more efficient in terms of NO_x removal. The plasma did not increase the removal efficiency at temperatures in excess of 250 °C, which could be attributed to the reactivity of the catalyst with *n*-heptane at these temperatures, as presented in Figure 4.

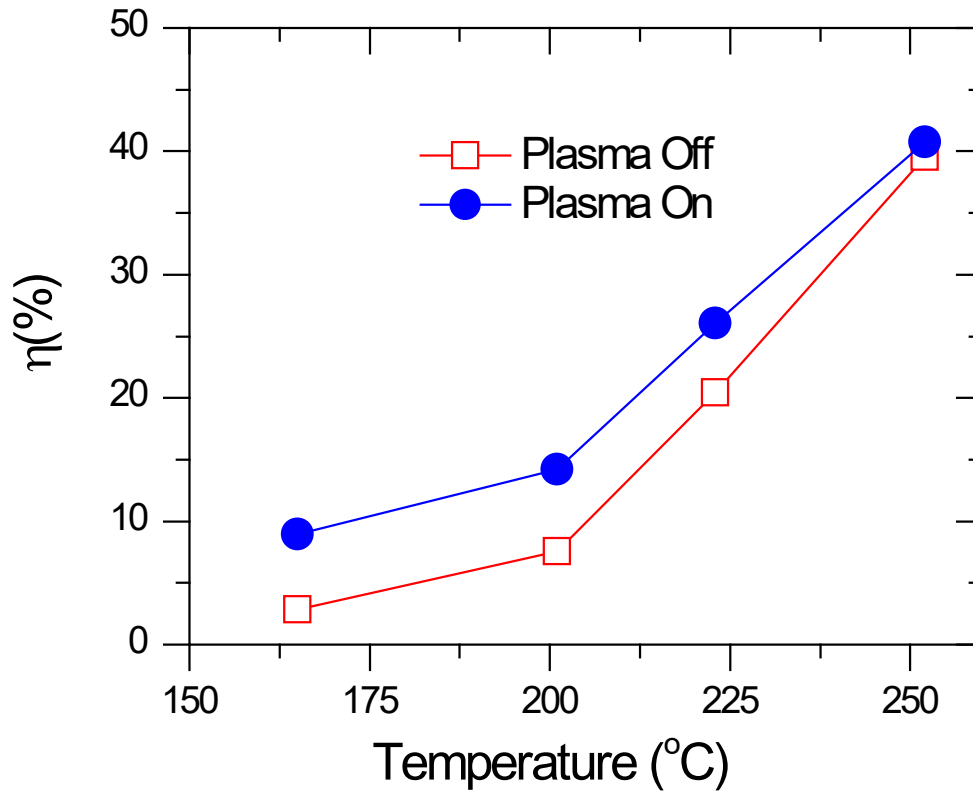


Figure 4.4. Enhancing the removal efficiency of NO_x at low temperatures by coupling the catalytic removal process with gliding arc plasma to generate oxygenated hydrocarbons from *n*-heptane ($\text{GHSV}=5000 \text{ h}^{-1}$; $\text{NO}_{\text{inlet}}=300 \text{ ppm}$; $n\text{-heptane}_{\text{inlet}}=386 \text{ ppm}$; water content=3.5 %; total flow rate=12 L/min in which 2 L/min with $\text{O}_2/\text{N}_2 = 1/9$ for plasma; input power $\sim 11 \text{ W}$; SEI of 55 J/L).

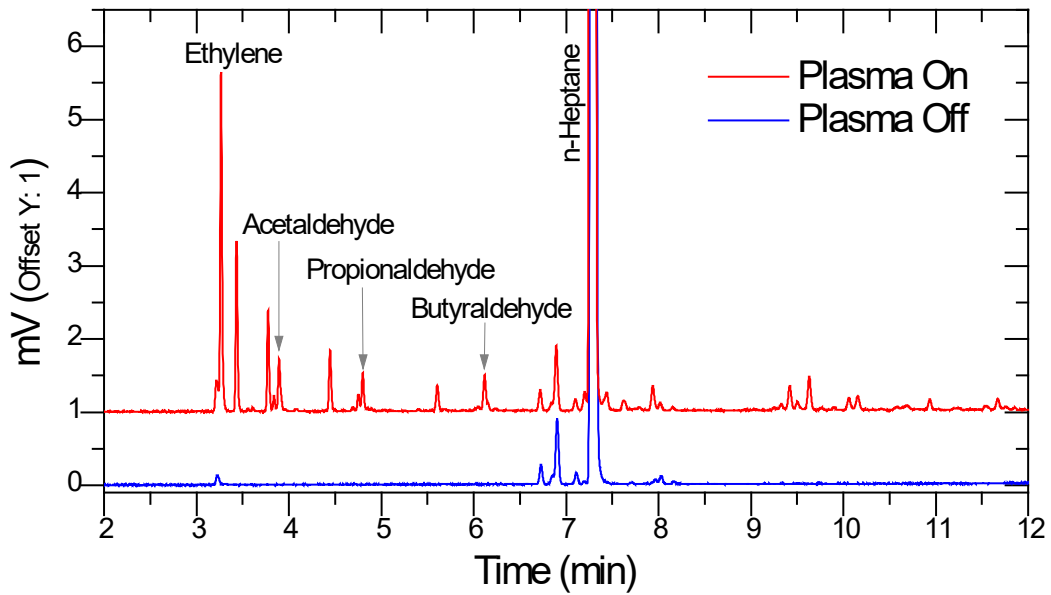


Figure 4.5. Chromatograms of gases produced in the gliding arc reactor at ~ 11 W input power (Flow rate of 2 L/min: $O_2/N_2=1/9$; $n\text{-heptane}_{inlet}=2314$ ppm that equilibrium to 386 ppm after diluting to 12 L/min).

4.3.2.2. Effect of input energy of plasma

Enhancing the removal efficiency of NO_x by injecting OHCs generated by GA plasma discharge would be possible with the formation of a higher concentration of OHCs, whereas the oxidation of the initial HC to CO_2 would be less complete. This suggests that the effect of the input energy of the plasma on the NO_x removal would be complex, contrary to the one-stage plasma-catalyst reaction for NO_x removal in which case the removal efficiency increased significantly along with the input energy.[58] The dependence of the removal efficiency of NO_x on the input energy of the GA plasma is plotted in Figure 9.

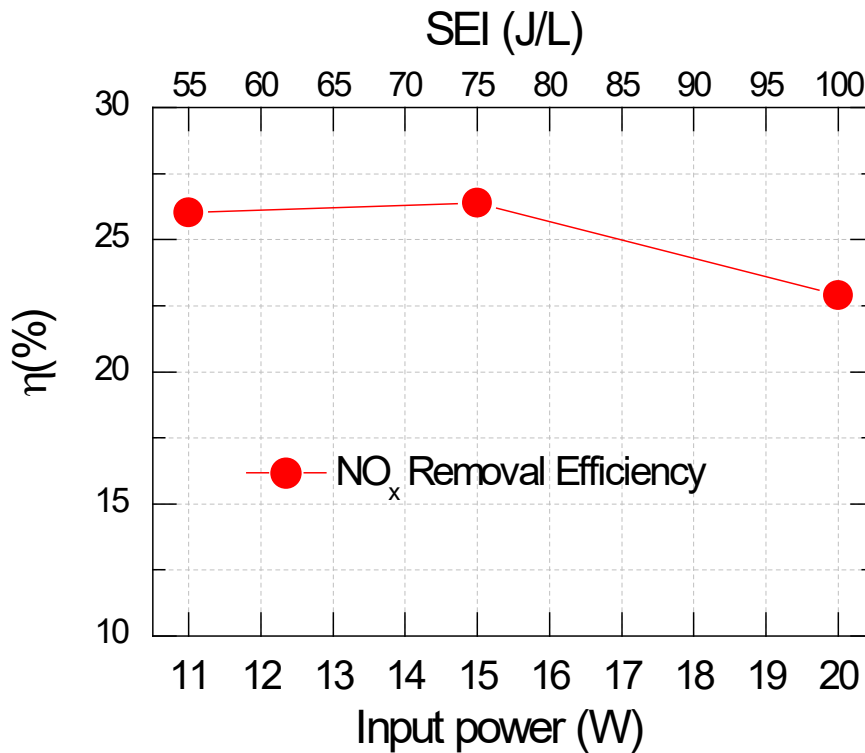


Figure 4.6. Effect of the input power on the removal efficiency of NO_x when the catalyst is operated at 223 °C (GHSV=5000 h⁻¹; NO_{inlet}=300 ppm; n-heptane_{inlet}=386 ppm; water content=3.5 %; total flow rate=12 L/min in which 2 L/min with O₂/N₂ =1/9 for plasma).

Figure 4.6 shows that the removal efficiency was maintained when the SEI ranged from 55 to 75 J/L, following which the efficiency decreased as the SEI increased to 100 J/L. Note that an SEI of 55 J/L was the minimum input energy necessary to stabilize the gliding arc plasma discharge at a gas flow rate of 2 L/min. Overall, a GA plasma discharge with a high input power negatively affects the removal efficiency of NO_x. To investigate these observations, the conversion of n-heptane and the formation of NO_x, CO₂, and O₃ during exposure to the GA plasma were monitored. Figure 4.7(a) shows that the formation of NO_x increased with increasing input power of the GA plasma. This suggested that the absolute amount of NO_x at the inlet of the catalyst stage is increased. Consequently, at high input power, the NO_x removal efficiency of the process would not be enhanced as a result of pretreatment

by the GA plasma. Preferably, exposure to the GA plasma should form OHCs; unfortunately, the complete oxidation of *n*-heptane still leads to the formation of CO₂ in the GA plasma. This suggests that it may be necessary to lower the C₁/N ratio in the feed gas; moreover, the degree of conversion increased as the input power increased, as shown in Figure 4.7(b). The presence of O₃ in the feed gas would improve the SCR of NO_x[113, 114] through the oxidization of NO to form NO₂ or HCs to form OHCs. The O₃ in the gas outlet of the GA plasma reactor was found to exist at trace levels, as measured by a 4–400 ppm detector tube (GASTEC Corp., no. 18M Ozone, Japan). The O₃/O₂, which were generated during GA plasma discharge, immediately reacted with NO and *n*-heptane, which can be considered the reason for the absence of O₃ at the outlet of the GA plasma reactor. The results are in line with those of previous work,[56] i.e., the absence of O₃ from the gas outlet of humid air plasma with *n*-heptane in the feed gas. Furthermore, the high temperature of the GA plasma is another reason for the lower amount of O₃ at the gas outlet.[115] Although the formation of more OHCs owing to the increased conversion of *n*-heptane at high input power has a positive effect on NO_x removal, the formation of NO_x and CO₂ during plasma discharge negatively affects the efficiency; overall, the removal efficiency of NO_x decreases when the input energy of the GA plasma is above 80 J/L.

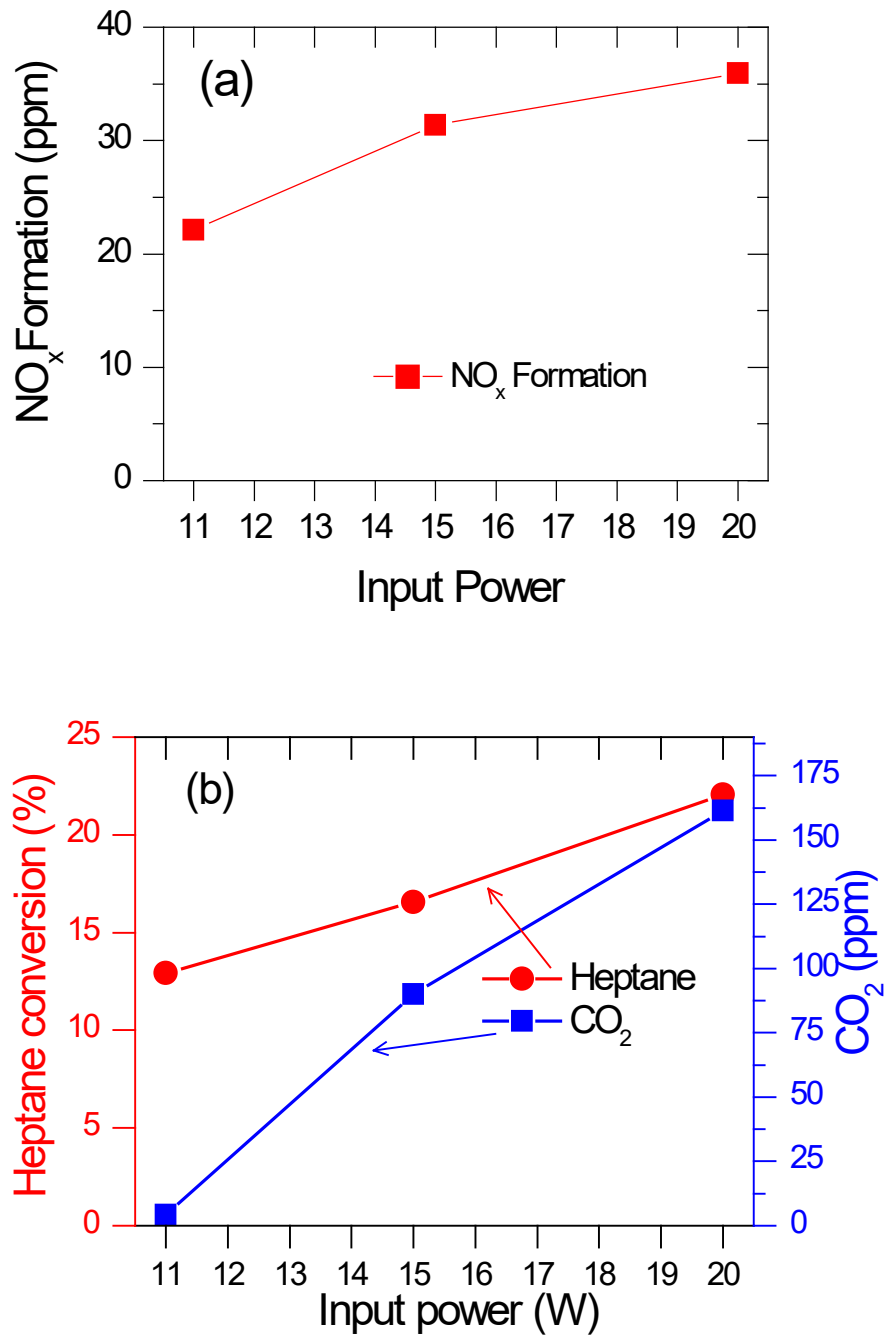


Figure 4.7. Effects of input power on the (a) formation of NO_x and (b) conversion of n-heptane and formation of CO₂ using gliding arc plasma (plasma flow rate = 2 L/min with O₂/N₂ = 1/9 and concentration of n-heptane = 2314 ppm; CO₂ and NO_x concentration were measured after diluting to 12 L/min).

4.3.3. Potential pretreatment of HC injection by plasma and future study

As mentioned above, the removal efficiency of NO_x as a result of pretreatment in the form of HC injection depends on the formation of NO_x in the GA plasma stage. To evaluate the effect of OHCs on enhancing the NO_x removal, the effect of lowering the absolute amount of NO_x on the removal efficiency of NO_x during the catalyst stage of the two-stage process (consisting of the plasma and the catalyst reactors, respectively) according to Eq. 2, is considered. As seen in Figure 4.8, the removal efficiency of NO_x in the catalyst stage was higher than that of the catalyst alone or the plasma catalyst under the same conditions. Partially, the absolute amount of NO_x is still lowered at 250 °C, whereas the difference between the removal efficiency of NO_x with the catalyst or plasma catalyst is insignificant. The removal efficiency of NO_x would be increased by increasing the ratio of the total flow rate to that of the plasma flow rate or lowering the amount of NO_x that forms. In a packed-bed catalyst reactor, the gas flow rate is limited because of the pressure drop and a honeycomb catalyst was proposed to overcome this problem.[116] In this study, the aforementioned flow rate ratio is fixed at 6 times, above which the fraction of NO_x formed by the GA plasma decreases when considering the overall plasma catalyst process; consequently, the removal efficiency would be significantly improved. Furthermore, a higher flow ratio requires a high inlet concentration of *n*-heptane in the plasma feed, which would result in the formation of less NO_x . Interestingly, the average energy consumption is significantly decreased as expressed by Eq. 5. As a result, the pretreatment of HCs by plasma increases the extent to which the absolute amount of NO_x is lowered by 5 to 10%. The use of a high ratio of the flow rate is suggested to increase the effect of the OHCs, yet it would lower the average energy consumption; this would be possible by using plasma in conjunction with a honeycomb catalyst.

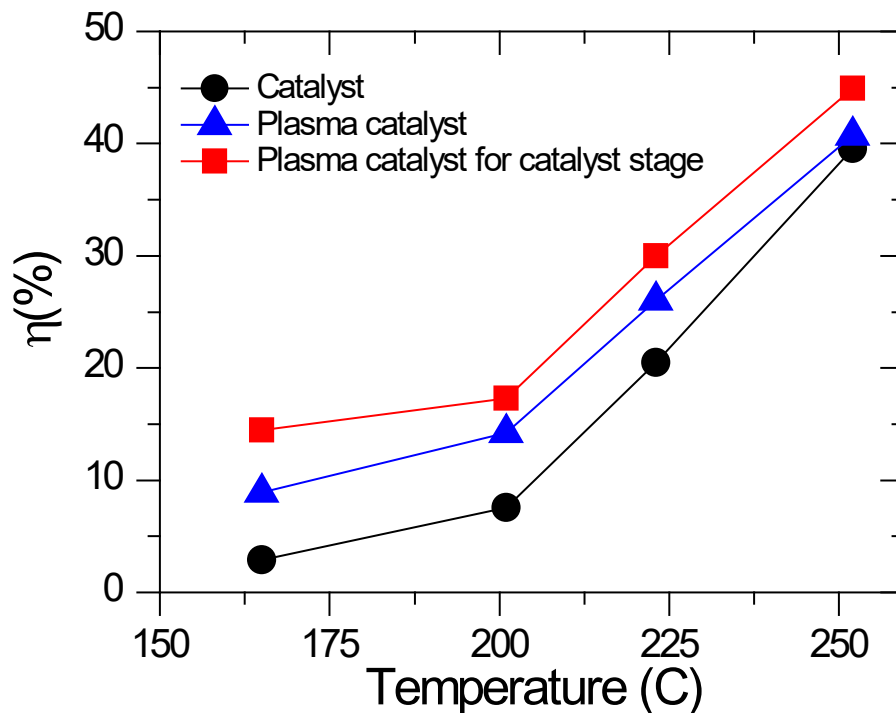


Figure 4.8. Comparison between the removal efficiency and absolute amount of NO_x reduced (GHSV = 5000 h^{-1} ; NO_{inlet} = 300 ppm; n -heptane $_{inlet}$ = 386 ppm; water content = 3.5 %; total flow rate = 12 L/min in which 2 L/min with $O_2/N_2 = 1/9$ for plasma; SIE = 55 J/L).

4.3.4. Analysis of optical emission spectra of the gliding arc plasma

The optical emissions from the GA plasma were recorded by optical emission spectroscopy (AvaSpec-2048 XL, Netherlands), as shown in Figure 4.9. These spectra are characteristic of the atmospheric pressure plasma described elsewhere.[117, 118] Briefly, the spectra of the GA plasma also consisted of intense lines of N_2 and N_2^+ in the second positive system of N_2 ($C^3\Pi_u \rightarrow B^3\Pi_g$) and the first negative system of N_2^+ ($B^2\Sigma_u^+ \rightarrow X^2\Sigma_g^+$), respectively. Similar to these previous reports, the OH lines at 296 and 306 nm are inseparable from the N_2 lines near these wavelengths owing to the strong intensity of the N_2 lines that overlap with the OH lines. In addition to this, the other emissions, those of NO, CH, C_2 , CO, were observed clearly. Specifically, the NO band in the γ system ($A^2\Sigma^+ \rightarrow X^2\Pi$) from 200 to

300 nm increased with the absence of *n*-heptane in the feed gas. The significant decrease in the NO emission with *n*-heptane in the plasma zone can be explained by its reaction with oxygen radicals to form OHCs. Meanwhile, a comparison between the spectra in the presence/absence of *n*-heptane indicated a CH band at 387 nm, and C₂ and CO in the range from 500 to 600 nm, as shown in the inset figure. Moreover, the oxygen line in the range [750–900] nm was observed clearly, owing to the strong plasma streamer with a sufficiently strong current. The OES analysis demonstrated that the gliding arc plasma consisted of energetic electrons, ions, radicals, and the excited species of gas molecules, all of which were responsible for the high conversion rates of *n*-heptane to form OHCs and even a small amount of CO₂ (although the latter only occurred at low temperatures).

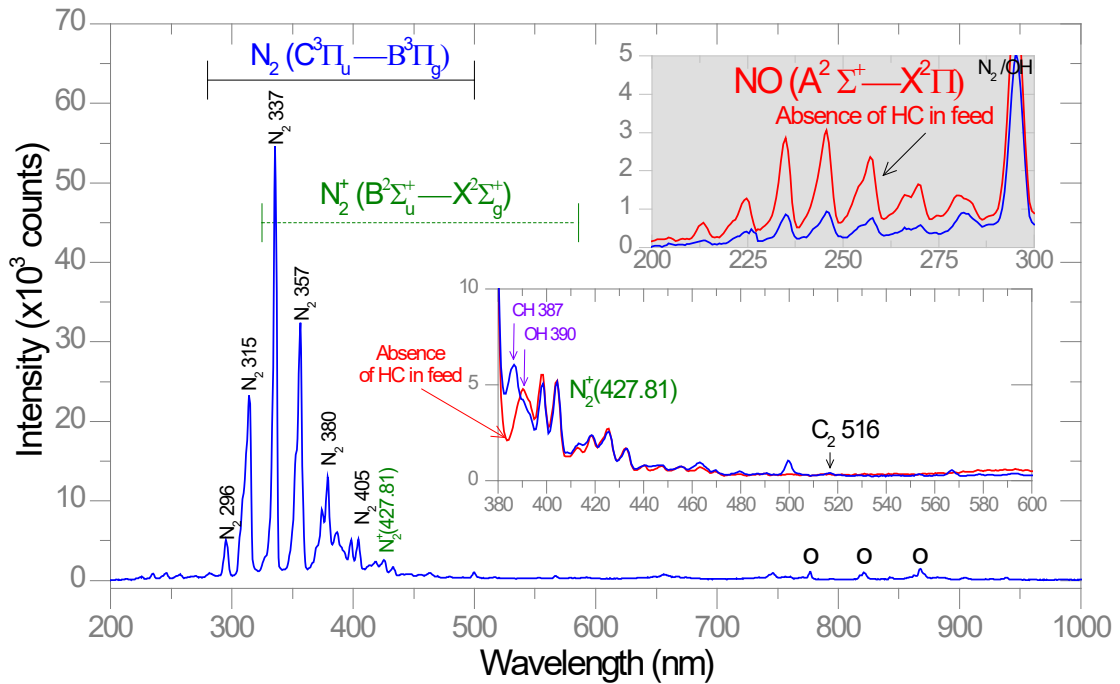


Figure 4.9. Optical emission spectra of gliding arc plasma at ED of 330 J/L (—, blue line) with *n*-heptane = 2314 ppm in the feed gas and (—, red line) without *n*-heptane in the feed gas (plasma flow rate = 2 L/min in with O₂/N₂ = 1/9).

4.4. Summary

The removal of NO_x over $\text{Ag}/\gamma\text{-Al}_2\text{O}_3$ with *n*-heptane as a reducing agent was investigated. The dependence of the NO_x removal efficiency on typical reducing agents, the temperature, and the amount of water in the feed was examined. Generally, the removal efficiency was increased as the temperature and C_1/N ratio increased. Interestingly, the result indicated that OHCs are more effective than HCs for NO_x removal in the low-temperature range. However, a large amount of water in the feed adversely affects NO_x removal with large amounts of water decreasing the removal efficiency. As the NO_x removal depends on typical reducing agents, the experimental data showed that the NO_x removal efficiency was increased significantly by pretreating the *n*-heptane flow with the GA plasma. This result is the consequence of mixtures of OHCs in the feed gas that were generated by pretreating the *n*-heptane flow with GA plasma. The formation of NO_x during exposure of the feed gas to the GA plasma results in the decrease in overall NO_x removal efficiency, and thus, the plasma pretreatment would become more effective when the ratio of the total flow rate to the plasma flow rate is high, just like actual diesel exhaust treatment.

CHAPTER 5 – GENERAL CONCLUSION

The main goal of this study was an improvement of the removal efficiency of VOC and NO_x by developing non-thermal plasma catalyst systems and optimizing various vital parameters. This study consists of two research works, and in each study, different types of homemade non-thermal plasma reactors are used to generate plasma at room temperature and atmospheric pressure.

The first work investigated the sandwich-type corona discharge plasma in a honeycomb monolith reactor to remove acetaldehyde. The effects of several essential working parameters, experimental conditions, and processes on the performance of acetaldehyde removal are examined. The main achievements of the experimental results are given as conclusions:

- ✓ Influence of metal catalyst: The results indicated that coating metal catalyst on the surface of the monolith has better performance than bare monolith on the increasing removal efficiency and effects to achieve high discharge power.
- ✓ Influence of flow rate: Acetaldehyde removal decreases with decreasing gas flow rate from 60 L/min to 20 L/min with keeping constant inlet acetaldehyde concentration at the same 25 J/L SEI.
- ✓ Influence of humidity: The results showed that moisture of the feed gas plays a crucial role in the acetaldehyde removal process. The removal efficiency of acetaldehyde decreased with an increasing water content of the feed gas at the same SEI. However, to obtain the same discharge power, the requirement of the applied voltage decreased in high humidified air.
- ✓ Influence of the inlet acetaldehyde concentration: In the range of 5-20 ppm inlet concentration of acetaldehyde, decreasing in the removal efficiency was negligible. Thus, the system can be usable in various conditions.

- ✓ A comparison of two methods: the study demonstrated that the energy consumption was very low in a plasma catalytic system compared to the thermal catalytic method.

The honeycomb discharge enables operating under humid conditions and high throughput of contaminated gas, suggesting that it is capable of practical plasma application for acetaldehyde removal.

The second work examined the PPC system, which consists of the gliding arc plasma reactor and γ -Al₂O₃ catalyst stages for NO_x removal. The rotational gliding arc plasma reactor was designed, constructed, and optimized to reform HC to OHCs. Several input parameters and conditions for the reduction of NO_x were also investigated. Various obtained vital research findings are as follows:

- ✓ The effect of the reducing agents on the deNO_x process at several temperatures is tested. The results indicated that OHCs are more effective than n-heptane as reductants in improving NO_x removal efficiency at low-temperature ranges (165-252 °C).
- ✓ The removal efficiency of NO_x increased with increasing C₁/N ratio, and a high amount of water content in the feed gas decreased the NO_x reduction.
- ✓ The results show that the gliding arc plasma can effectively reform HC to OHCs, for instance, acetaldehyde, butyraldehyde, and propionaldehyde. These OHCs enhanced the NO_x conversion rate by around 10 % at low temperatures. Additionally, there is a cost-effective aspect: there is no need to use any other chemical such as urea or ammonia as a reductant in this method because the diesel fuel can be useable as a reducing agent from an automobile's fuel tank instead of n-heptane.

Suggests that the removal efficiency of the NO_x will increase by this method when increasing the fraction ratio between the total flow rate and flow rate of the carrier gas of the gliding arc reactor because of the increase in the injection of n-heptane to the GA reactor. As a result, there is less chance of producing NO_x in the GA plasma reactor, and the NO_x reduction can be improved enough in the catalyst stage.

BIBLIOGRAPHY

- [1] M. Maione, E. Mocca, K. Eisfeld, Y. Kazepov, S. Fuzzi, Public perception of air pollution sources across Europe, *Ambio* 50 (2021) 1150-1158.
- [2] M.C. Turner, Z.J. Andersen, A. Baccarelli, W.R. Diver, S.M. Gapstur, C.A. Pope III, D. Prada, J. Samet, G. Thurston, A. Cohen, Outdoor air pollution and cancer: An overview of the current evidence and public health recommendations, *CA: a cancer journal for clinicians* 70 (2020) 460-479.
- [3] C. He, J. Cheng, X. Zhang, M. Douthwaite, S. Patisson, Z. Hao, Recent Advances in the Catalytic Oxidation of Volatile Organic Compounds: A Review Based on Pollutant Sorts and Sources, *Chem. Rev.* 119 (2019) 4471-4568.
- [4] M. Gao, W. Liu, H. Wang, X. Shao, A. Shi, X. An, G. Li, L. Nie, Emission factors and characteristics of volatile organic compounds (VOCs) from adhesive application in indoor decoration in China, *Sci. Total Environ.* 779 (2021) 145169.
- [5] D.A. Sarigiannis, S.P. Karakitsios, A. Gotti, I.L. Liakos, A. Katsoyiannis, Exposure to major volatile organic compounds and carbonyls in European indoor environments and associated health risk, *Environment International* 37 (2011) 743-765.
- [6] C. Klett, X. Duten, S. Tieng, S. Touchard, P. Jestin, K. Hassouni, A. Vega-González, Acetaldehyde removal using an atmospheric non-thermal plasma combined with a packed bed: Role of the adsorption process, *J. Hazard. Mater.* 279 (2014) 356-364.
- [7] M. Hadei, A. Shahsavani, P.K. Hopke, M. Kermani, M. Yarahmadi, B. Mahmoudi, Comparative health risk assessment of in-vehicle exposure to formaldehyde and

acetaldehyde for taxi drivers and passengers: Effects of zone, fuel, refueling, vehicle's age and model, *Environ. Pollut.* 254 (2019) 112943.

[8] P. Gustafson, L. Barregard, B. Strandberg, G. Sällsten, The impact of domestic wood burning on personal, indoor and outdoor levels of 1,3-butadiene, benzene, formaldehyde and acetaldehyde, *J. Environ. Monit.* 9 (2007) 23-32.

[9] S. Vardoulakis, E. Giagloglou, S. Steinle, A. Davis, A. Sleeuwenhoek, K.S. Galea, K. Dixon, J.O. Crawford, Indoor Exposure to Selected Air Pollutants in the Home Environment: A Systematic Review, *International Journal of Environmental Research and Public Health* 17 (2020) 8972.

[10] S. Vardoulakis, P. Kinney, Grand challenges in sustainable cities and health, *Frontiers in Sustainable Cities* (2019) 7.

[11] Y. Lei, C. Qin, T. Qiu, G. Yue, M. Ding, NO_x Emission Removal from a Parallel Diesel Engine Group by SCR System Based on Distributed Control Technology, *Environ. Sci. Technol.* 55 (2021) 6352-6362.

[12] N. Sharma, A.K. Agarwal, P. Eastwood, T. Gupta, A.P. Singh, Introduction to Air Pollution and Its Control, in: N. Sharma, A.K. Agarwal, P. Eastwood, T. Gupta, A.P. Singh (Eds.) *Air Pollution and Control*, Springer Singapore, Singapore, 2018, pp. 3-7.

[13] P. Ni, X. Wang, H. Li, A review on regulations, current status, effects and reduction strategies of emissions for marine diesel engines, *Fuel* 279 (2020) 118477.

[14] N.M. Liu, J. Grigg, Diesel, children and respiratory disease, *BMJ Paediatr Open* 2 (2018) e000210-e000210.

- [15] L.B. Weger, J. Leitão, M.G. Lawrence, Expected impacts on greenhouse gas and air pollutant emissions due to a possible transition towards a hydrogen economy in German road transport, *Int. J. Hydrogen Energy* 46 (2021) 5875-5890.
- [16] A. Razmjoo, L. Gakenia Kaigutha, M.A. Vaziri Rad, M. Marzband, A. Davarpanah, M. Denai, A Technical analysis investigating energy sustainability utilizing reliable renewable energy sources to reduce CO₂ emissions in a high potential area, *Renewable Energy* 164 (2021) 46-57.
- [17] Z. Xu, Y. Li, H. Shi, Y. Lin, Y. Wang, Q. Wang, T. Zhu, Application Prospect of K Used for Catalytic Removal of NO_x, CO_x, and VOCs from Industrial Flue Gas: A Review, *Catal.* 11 (2021) 419.
- [18] J. Van Durme, J. Dewulf, C. Leys, H. Van Langenhove, Combining non-thermal plasma with heterogeneous catalysis in waste gas treatment: A review, *Appl. Catal. B: Environ.* 78 (2008) 324-333.
- [19] S. K. P. Veerapandian, N. De Geyter, J.-M. Giraudon, J.-F. Lamonier, R. Morent, The Use of Zeolites for VOCs Abatement by Combining Non-Thermal Plasma, Adsorption, and/or Catalysis: A Review, *Catal.* 9 (2019) 98.
- [20] C. Klett, S. Touchard, A. Vega-Gonzalez, M. Redolfi, X. Bonnin, K. Hassouni, X. Duten, Experimental and modeling study of the oxidation of acetaldehyde in an atmospheric-pressure pulsed corona discharge, *Plasma Sources Sci. Technol.* 21 (2012) 045001.
- [21] A. Lejeune, A. Cabrol, R. Lebullenger, A. Denicourt-Nowicki, A. Roucoux, A. Couvert, P.-F. Biard, Novel and Sustainable Catalytic Ruthenium-Doped Glass Foam for

Thermocatalytic Oxidation of Volatile Organic Compounds: An Experimental and Modeling Study, *Ind. Eng. Chem. Res.* 59 (2020) 14758-14766.

[22] P.H. Affonso Nóbrega, V. Rohani, L. Fulcheri, Non-thermal plasma treatment of volatile organic compounds: A predictive model based on experimental data analysis, *Chem. Eng. J.* 364 (2019) 37-44.

[23] G.R. Parmar, N. Rao, Emerging control technologies for volatile organic compounds, *Crit. Rev. Evn. Sci. Tec.* 39 (2008) 41-78.

[24] L. Han, S. Cai, M. Gao, J.-y. Hasegawa, P. Wang, J. Zhang, L. Shi, D. Zhang, Selective catalytic reduction of NO_x with NH₃ by using novel catalysts: State of the art and future prospects, *Chem. Rev.* 119 (2019) 10916-10976.

[25] A.B. Ngo, T.H. Vuong, H. Atia, U. Bentrup, V.A. Kondratenko, E.V. Kondratenko, J. Rabeah, U. Ambruster, A. Brückner, Effect of formaldehyde in selective catalytic reduction of NO_x by Ammonia (NH₃-SCR) on a commercial V₂O₅-WO₃/TiO₂ catalyst under model conditions, *Environ. Sci. Technol.* 54 (2020) 11753-11761.

[26] Y. Jung, Y.J. Shin, Y.D. Pyo, C.P. Cho, J. Jang, G. Kim, NO_x and N₂O emissions over a Urea-SCR system containing both V₂O₅-WO₃/TiO₂ and Cu-zeolite catalysts in a diesel engine, *Chem. Eng. J.* 326 (2017) 853-862.

[27] A.M. Beale, F. Gao, I. Lezcano-Gonzalez, C.H.F. Peden, J. Szanyi, Recent advances in automotive catalysis for NO_x emission control by small-pore microporous materials, *Chem. Soc. Rev.* 44 (2015) 7371-7405.

[28] S. Mohan, P. Dinesha, S. Kumar, NO_x reduction behaviour in copper zeolite catalysts for ammonia SCR systems: A review, *Chem. Eng. J.* 384 (2020) 123253.

[29] L. Zhang, Q. Wu, X. Meng, U. Müller, M. Feyen, D. Dai, S. Maurer, R. McGuire, A. Moini, A.-N. Parvulescu, W. Zhang, C. Shi, T. Yokoi, X. Pan, X. Bao, H. Gies, B. Marler, D.E. De Vos, U. Kolb, F.-S. Xiao, Recent advances in the preparation of zeolites for the selective catalytic reduction of NO_x in diesel engines, *React. Chem. Eng.* 10.1039/c8re00214b (2019).

[30] J. Xu, H. Wang, F. Guo, C. Zhang, J. Xie, Recent advances in supported molecular sieve catalysts with wide temperature range for selective catalytic reduction of NO_x with C₃H₆, *RSC Adv.* 9 (2019) 824-838.

[31] C. Jia, J. Gao, K.W. Huang, V. Jose, P. Thepsithar, J.-M. Lee, Selective catalytic reduction of NO_x in marine engine exhaust gas over supported transition metal oxide catalysts, *Chem. Eng. J.* 414 (2021) 128794.

[32] W. Lu, Y. Abbas, M.F. Mustafa, C. Pan, H. Wang, A review on application of dielectric barrier discharge plasma technology on the abatement of volatile organic compounds, *Front. Environ. Sci. Eng.* 13 (2019) 1-19.

[33] M.e. Grabchenko, N. Mikheeva, G. Mamontov, M. Salaev, L. Liotta, O. Vodyankina, Ag/CeO₂ composites for catalytic abatement of CO, soot and VOCs, *Catal.* 8 (2018) 285.

[34] H.H. Kim, Nonthermal plasma processing for air-pollution control: a historical review, current issues, and future prospects, *Plasma Process. Polym.* 1 (2004) 91-110.

[35] A. Fridman, A. Chirokov, A. Gutsol, Non-thermal atmospheric pressure discharges, *J. Phys. D: Appl. Phys.* 38 (2005) R1.

- [36] X. Tu, J.C. Whitehead, T. Nozaki, Plasma Catalysis: Fundamentals and Applications, Springer, Cham, Springer Nature Switzerland AG 2019, 2019.
- [37] A. Fridman, L.A. Kennedy, Plasma physics and engineering, second edition ed., CRC press, 2011.
- [38] C. Niu, J. Niu, S. Wang, Z. Wang, S. Dong, H. Fan, Y. Hong, D. Liu, Synergistic effect in one-stage dielectric barrier discharge plasma and Ag/Al₂O₃ catalytic systems on C₂H₂-SCR of NO_x, Catal. Commun. 123 (2019) 49-53.
- [39] A. Khacef, P. Da Costa, Plasma-Catalytic Removal of NO_x in Mobile and Stationary Sources, Plasma Catalysis (2019) 115-144.
- [40] Z. Bai, Z. Zhang, B. Chen, Q. Zhao, M. Crocker, C. Shi, Non-thermal plasma enhanced NSR performance over Pt/M/Ba/Al₂O₃ (M= Mn, Co, Cu) catalysts, Chem. Eng. J. 314 (2017) 688-699.
- [41] A. Khacef, P. Da Costa, Plasma-Catalytic Removal of NO_x in Mobile and Stationary Sources, in: X. Tu, J.C. Whitehead, T. Nozaki (Eds.) Plasma Catalysis: Fundamentals and Applications, Springer International Publishing, Cham, 2019, pp. 115-144.
- [42] Z. Bai, Z. Zhang, B. Chen, Q. Zhao, M. Crocker, C. Shi, Non-thermal plasma enhanced NSR performance over Pt/M/Ba/Al₂O₃ (M=Mn, Co, Cu) catalysts, Chem. Eng. J. 314 (2017) 688-699.
- [43] S. Li, X. Dang, X. Yu, G. Abbas, Q. Zhang, L. Cao, The application of dielectric barrier discharge non-thermal plasma in VOCs abatement: A review, Chem. Eng. J. 388 (2020) 124275.

- [44] P. Cools, N. De Geyter, R. Morent, Plasma-Catalytic Removal of VOCs, in: X. Tu, J.C. Whitehead, T. Nozaki (Eds.) Plasma Catalysis: Fundamentals and Applications, Springer International Publishing, Cham, 2019, pp. 145-180.
- [45] X. Feng, H. Liu, C. He, Z. Shen, T. Wang, Synergistic effects and mechanism of a non-thermal plasma catalysis system in volatile organic compound removal: a review, Catal. Sci. Technol. 8 (2018) 936-954.
- [46] A. Mizuno, M. Craven, Plasma Catalysis Systems, in: X. Tu, J.C. Whitehead, T. Nozaki (Eds.) Plasma Catalysis: Fundamentals and Applications, Springer International Publishing, Cham, 2019, pp. 21-46.
- [47] S. Saud, D.B. Nguyen, R.M. Bhattarai, N. Matyakubov, I. Heo, Y.S. Mok, Dependence of plasma discharge performance in commercial honeycomb monoliths on the reactor configuration and key parameters, Plasma Sources Sci. Technol. (2020) Submitted.
- [48] D.B. Nguyen, S. Saud, M.M. Hossain, I. Heo, Y.S. Mok, Generation of atmospheric pressure plasma in honeycomb monolith, Chem. Eng. J. (2020) Submitted.
- [49] M. Okubo, T. Kuroki, T. Yamamoto, S. Miwa, Soot incineration of diesel particulate filter using honeycomb nonthermal plasma, SAE Trans. 112 (2003) 1561-1567.
- [50] M. Okubo, T. Kuroki, Y. Miyairi, T. Yamamoto, Low-temperature soot incineration of diesel particulate filter using remote nonthermal plasma induced by a pulsed barrier discharge, IEEE Trans. Ind. Appl. 40 (2004) 1504-1512.
- [51] K. Hensel, S. Katsura, A. Mizuno, DC microdischarges inside porous ceramics, IEEE Trans. Plasma Sci. 33 (2005) 574-575.

[52] K. Hensel, V. Martišovič, Z. Machala, M. Janda, M. Leštinský, P. Tardiveau, A. Mizuno, Electrical and optical properties of AC microdischarges in porous ceramics, *Plasma Process. Polym.* 4 (2007) 682-693.

[53] M. Okubo, N. Arita, T. Kuroki, T. Yamamoto, Carbon particulate matter incineration in diesel engine emissions using indirect nonthermal plasma processing, *Thin Solid Films* 515 (2007) 4289-4295.

[54] K. Hensel, Microdischarges in ceramic foams and honeycombs, *The European Physical Journal D* 54 (2009) 141.

[55] W.S. Kang, D.H. Lee, J.-O. Lee, M. Hur, Y.-H. Song, Combination of plasma with a honeycomb-structured catalyst for automobile exhaust treatment, *Environ. Sci. Technol.* 47 (2013) 11358-11362.

[56] D.B. Nguyen, N. Matyakubov, S. Saud, I.J. Heo, S.-J. Kim, Y.J. Kim, J.H. Lee, Y.S. Mok, High-Throughput NO_x Removal by Two-Stage Plasma Honeycomb Monolith Catalyst, *Environ. Sci. Technol.* 55 (2021) 6386-6396.

[57] J.B. Lee, H.-C. Kang, O.J. Jo, S.Y. Mok, Consideration of the role of plasma in a plasma-coupled selective catalytic reduction of nitrogen oxides with a hydrocarbon reducing agent, *Catal.* 7 (2017) 325.

[58] D.B. Nguyen, I.J. Heo, Y.S. Mok, Enhanced performance at an early state of hydrocarbon selective catalyst reduction of NO_x by atmospheric pressure plasma, *J. Ind. Eng. Chem.* 68 (2018) 372-379.

- [59] J. Zhu, J. Gao, Z. Li, A. Ehn, M. Aldén, A. Larsson, Y. Kusano, Sustained diffusive alternating current gliding arc discharge in atmospheric pressure air, *Appl. Phys. Lett.* 105 (2014) 234102.
- [60] A. Bogaerts, E. Neyts, R. Gijbels, J. Van der Mullen, Gas discharge plasmas and their applications, *Spectrochim. Acta B* 57 (2002) 609-658.
- [61] J. Meichsner, M. Schmidt, R. Schneider, H.E. Wagner, Nonthermal plasma chemistry and physics, CRC Press, 2012.
- [62] A. Fridman, Plasma chemistry, Cambridge University Press, 2008.
- [63] R. d'Agostino, P. Favia, Y. Kawai, H. Ikegami, N. Sato, F. Arefi-Khonsari, Advanced plasma technology, John Wiley & Sons, 2008.
- [64] F.F. Chen, Introduction to plasma physics, Springer Science & Business Media, 2012.
- [65] R.J. Goldston, Introduction to plasma physics, CRC Press, 2020.
- [66] G. Petitpas, J.D. Rollier, A. Darmon, J. Gonzalez-Aguilar, R. Metkemeijer, L. Fulcheri, A comparative study of non-thermal plasma assisted reforming technologies, *Int. J. Hydrogen Energy* 32 (2007) 2848-2867.
- [67] M.I. Boulos, P. Fauchais, E. Pfender, Thermal plasmas: fundamentals and applications, Springer Science & Business Media, 2013.
- [68] P.K. Chu, X. Lu, Low temperature plasma technology: Methods and applications, CRC Press, 2013.

- [69] K. Fricke, Influence of Non-thermal Plasma-based Biological Decontamination Processes on the Surface Properties of Plasma-exposed Polymers.
- [70] J.E. Harry, Introduction to plasma technology: science, engineering, and applications, John Wiley & Sons, 2013.
- [71] S. Manahan, Environmental chemistry, CRC press, 2017.
- [72] S.E. Manahan, Environmental science and technology: a sustainable approach to green science and technology, CRC Press, 2006.
- [73] P. Grennfelt, A. Engleryd, M. Forsius, Ø. Hov, H. Rodhe, E. Cowling, Acid rain and air pollution: 50 years of progress in environmental science and policy, *Ambio* 49 (2020) 849-864.
- [74] G.H. Bernhard, R.E. Neale, P.W. Barnes, P. Neale, R.G. Zepp, S.R. Wilson, A.L. Andrady, A.F. Bais, R. McKenzie, P. Aucamp, Environmental effects of stratospheric ozone depletion, UV radiation and interactions with climate change: UNEP Environmental Effects Assessment Panel, update 2019, *Photochemical & Photobiological Sciences* 19 (2020) 542-584.
- [75] Z. Abd Allah, Non-thermal atmospheric pressure plasma for remediation of volatile organic compounds, The University of Manchester (United Kingdom), 2012.
- [76] C. Du, X. Gong, Y. Lin, Decomposition of volatile organic compounds using corona discharge plasma technology, *Journal of the Air & Waste Management Association* 69 (2019) 879-899.
- [77] J.R. Roth, Industrial plasma engineering: Volume 2: Applications to nonthermal plasma processing, CRC press, 2001.

- [78] J. Meichsner, M. Schmidt, R. Schneider, H.E. Wagner, Nonthermal plasma chemical processes of general interest, *Nonthermal plasma chemistry and physics*, CRC Press, 2012, pp. 7-14.
- [79] A. Mizuno, Generation of non-thermal plasma combined with catalysts and their application in environmental technology, *Catal. Today* 211 (2013) 2-8.
- [80] S. Saud, D.B. Nguyen, S.-G. Kim, H.W. Lee, S.B. Kim, Y.S. Mok, Improvement of ethylene removal performance by adsorption/oxidation in a pin-type corona discharge coupled with Pd/ZSM-5 catalyst, *Catal.* 10 (2020) 133.
- [81] H. Zhang, X.D. Li, Y.Q. Zhang, T. Chen, J.H. Yan, C.M. Du, Rotating Gliding Arc Codriven by Magnetic Field and Tangential Flow, *IEEE Trans. Plasma Sci.* 40 (2012) 3493-3498.
- [82] A. Fridman, A. Gutsol, S. Gangoli, Y. Ju, T. Ombrello, Characteristics of Gliding Arc and Its Application in Combustion Enhancement, *J. Propul. Power* 24 (2008) 1216-1228.
- [83] S. Van Alphen, F. Jardali, J. Creel, G. Trenchev, R. Snyders, A. Bogaerts, Sustainable gas conversion by gliding arc plasmas: a new modelling approach for reactor design improvement, *Sustainable Energy & Fuels* 5 (2021) 1786-1800.
- [84] A. Fridman, S. Nester, L.A. Kennedy, A. Saveliev, O. Mutaf-Yardimci, Gliding arc gas discharge, *Prog. Energy Combust. Sci.* 25 (1999) 211-231.
- [85] S. Hu, B. Wang, Y. Lv, W. Yan, Conversion of methane to C₂ hydrocarbons and hydrogen using a gliding arc reactor, *Plasma Sci. Technol.* 15 (2013) 555.

- [86] A. Indarto, D.R. Yang, J.-W. Choi, H. Lee, H.K. Song, Gliding arc plasma processing of CO₂ conversion, *J. Hazard. Mater.* 146 (2007) 309-315.
- [87] Y.-j. LÜ, W.-j. YAN, S.-h. HU, B.-w. WANG, Hydrogen production by methanol decomposition using gliding arc gas discharge, *Journal of Fuel Chemistry and Technology* 40 (2012) 698-706.
- [88] A. Czernichowski, Gliding arc: applications to engineering and environment control, *Pure Appl. Chem.* 66 (1994) 1301-1310.
- [89] A. Indarto, J.-W. Choi, H. Lee, H. Keun Song, Treatment of dichloromethane using gliding arc plasma, *International journal of green energy* 3 (2006) 309-321.
- [90] B. Wang, Y. Cheng, C. Wang, J. Zou, Steam reforming of methane in a gliding arc discharge reactor to produce hydrogen and its chemical kinetics study, *Chem. Eng. Sci.* 253 (2022) 117560.
- [91] N. Matyakubov, D.B. Nguyen, S. Saud, Y.S. Mok, Enhancing the Selective Catalytic Reduction of NO_x at Low Temperature by Pretreatment of Hydrocarbons in a Gliding Arc Plasma, *Ind. Eng. Chem. Res.* 10.1021/acs.iecr.2c00025 (2022).
- [92] K. Pornmai, A. Jindanin, H. Sekiguchi, S. Chavadej, Synthesis gas production from CO₂-containing natural gas by combined steam reforming and partial oxidation in an AC gliding arc discharge, *Plasma Chem. Plasma Process.* 32 (2012) 723-742.
- [93] Q.H. Trinh, D.K. Dinh, D.H. Lee, D.B. Nguyen, Y.S. Mok, W.G. Lee, 12 - Combination of atmospheric pressure plasma with catalysts for dry reforming of methane to value-added chemicals, in: S. Nanda, D.-V. Vo (Eds.) *Innovations in Thermochemical Technologies for Biofuel Processing*, Elsevier, 2022, pp. 273-312.

[94] D.B. Nguyen, S. Saud, N. Matyakubov, Y.S. Mok, S. Ryu, H. Jeon, S.B. Kim, Propagation of humidified air plasma in a sandwich-type honeycomb plasma reactor and its dependence on the ambient temperature and reactor diameter, *Plasma Sources Sci. Technol.* 29 (2020) 125016.

[95] J. Manion, R. Huie, R. Levin, D. Burgess Jr, V. Orkin, W. Tsang, W. McGivern, J. Hudgens, V. Knyazev, D. Atkinson, E. Chai, A. Tereza, C. Lin, T. Allison, W. Mallard, F. Westley, J. Herron, R.F. Hampson, D. Frizzell, NIST Chemical Kinetics Database, Standard Reference Database 17, Version 7.0 (Web Version), Release 1.6.8 Data Version 2015.09, National Institute of Standards and Technology, Gaithersburg, Maryland, 20899-8320, Web address: <http://kinetics.nist.gov/>, 2019.

[96] T. Chang, J. Lu, Z. Shen, B. Zhang, Y. Huang, J. Cao, H. Liu, S.K.P. Veerapandian, N. De Geyter, R. Morent, Post Plasma Catalysis for the Removal of Acetaldehyde Using Mn–Co/HZSM-5 Catalysts, *Ind. Eng. Chem. Res.* 58 (2019) 14719-14728.

[97] X. Zhu, X. Gao, C. Zheng, Z. Wang, M. Ni, X. Tu, Plasma-catalytic removal of a low concentration of acetone in humid conditions, *RSC Adv.* 4 (2014) 37796-37805.

[98] R.W.B. Pearse, A.G. Gaydon, *The identification of molecular spectra*, 4th ed., Chapman and Hall, London, 1976.

[99] D.B. Nguyen, Q.H. Trinh, Y.S. Mok, W.G. Lee, Generation of cold atmospheric plasma jet by a coaxial double dielectric barrier reactor, *Plasma Sources Sci. Technol.* 29 (2020) 035014.

[100] Y.S. Mok, S.G. Kim, D.B. Nguyen, Q.H. Trinh, H.W. Lee, S.B. Kim, Plasma-catalytic oxidation of ethylene over zeolite-supported catalysts to improve the storage stability of agricultural products, *Catal. Today* 337 (2019) 208-215.

[101] A. Vega-González, X. Duten, S. Sauce, Plasma-Catalysis for Volatile Organic Compounds Decomposition: Complexity of the Reaction Pathways during Acetaldehyde Removal, *Catal.* 10 (2020) 1146.

[102] Z. Jia, M. Ben Amar, D. Yang, O. Brinza, A. Kanaev, X. Duten, A. Vega-González, Plasma catalysis application of gold nanoparticles for acetaldehyde decomposition, *Chem. Eng. J.* 347 (2018) 913-922.

[103] Z. Jia, A. Vega-Gonzalez, M.B. Amar, K. Hassouni, S. Tieng, S. Touchard, A. Kanaev, X. Duten, Acetaldehyde removal using a diphasic process coupling a silver-based nano-structured catalyst and a plasma at atmospheric pressure, *Catal. Today* 208 (2013) 82-89.

[104] M.E. Prudich, H. Chen, T. Gu, R.B. Gupta, K.P. Johnston, H. Lutz, G. Ma, Z. Su, Perry's chemical engineers' handbook, Section 2 physical and chemical data, McGraw-Hill Publishing, 2008.

[105] Y.R. Luo, Bond dissociation energies, in: D.R. Lide (Ed.) *CRC Handbook of Chemistry and Physics*, 90th Edition (Internet Version 2010), CRC Press/Taylor and Francis: Boca Raton, FL, 2010, pp. 9.64-97.

[106] C. Xu, W. Sun, L. Cao, T. Li, X. Cai, J. Yang, Highly efficient Pd-doped aluminate spinel catalysts with different divalent cations for the selective catalytic reduction of NO with H₂ at low temperature, *Chem. Eng. J.* 308 (2017) 980-987.

[107] M. Machida, S. Ikeda, D. Kurogi, T. Kijima, Low temperature catalytic NO_x-H₂ reactions over Pt/TiO₂-ZrO₂ in an excess oxygen, *Appl. Catal. B: Environ.* 35 (2001) 107-116.

[108] M.K. Kim, P.S. Kim, H.J. Kwon, I.-S. Nam, B.K. Cho, S.H. Oh, Simulation of OHC/SCR process over Ag/Al₂O₃ catalyst for removing NO_x from diesel engine, *Chem. Eng. J.* 209 (2012) 280-292.

[109] K. Arve, F. Klingstedt, K. Eränen, J. Wärnå, L.E. Lindfors, D.Y. Murzin, Kinetics of NO_x reduction over Ag/alumina by higher hydrocarbon in excess of oxygen, *Chem. Eng. J.* 107 (2005) 215-220.

[110] P. Talebizadeh, M. Babaie, R. Brown, H. Rahimzadeh, Z. Ristovski, M. Arai, The role of non-thermal plasma technique in NO_x treatment: A review, *Renewable Sustainable Energy Rev.* 40 (2014) 886-901.

[111] H. Wang, X. Li, M. Chen, X. Zheng, The effect of water vapor on NO_x storage and reduction in combination with plasma, *Catal. Today* 211 (2013) 66-71.

[112] A.V. Salker, M.S.F. Desai, Catalytic activity and mechanistic approach of NO reduction by CO over M_{0.05}Co_{2.95}O₄ (M=Rh, Pd & Ru) spinel system, *Appl. Surf. Sci.* 389 (2016) 344-353.

[113] T. Kuwahara, K. Yoshida, K. Hanamoto, K. Sato, T. Kuroki, M. Okubo, A Pilot-Scale Experiment for Total Marine Diesel Emission Control Using Ozone Injection and Nonthermal Plasma Reduction, *IEEE Trans. Ind. Appl.* 51 (2015) 1168-1178.

[114] T. Kuwahara, K. Yoshida, T. Kuroki, K. Hanamoto, K. Sato, M. Okubo, Pilot-scale combined reduction of accumulated particulate matter and NO_x using nonthermal plasma for marine diesel engine, *IEEE Trans. Ind. Appl.* 56 (2020) 1804-1814.

[115] H. Itoh, M. Taguchi, S. Suzuki, Thermal decomposition of ozone at high temperature leading to ozone zero phenomena, *J. Phys. D: Appl. Phys.* 53 (2020) 185206.

[116] S. Hosseini, H. Moghaddas, S. Masoudi Soltani, S. Kheawhom, Technological applications of honeycomb monoliths in environmental processes: A review, *Process Saf. Environ. Prot.* 133 (2020) 286-300.

[117] D.B. Nguyen, W.G. Lee, Effects of ambient gas on cold atmospheric plasma discharge in the decomposition of trifluoromethane, *RSC Adv.* 6 (2016) 26505-26513.

[118] N. Matyakubov, D.B. Nguyen, S. Saud, I. Heo, S.-J. Kim, Y.J. Kim, J.H. Lee, Y.S. Mok, Effective practical removal of acetaldehyde by a sandwich-type plasma-in-honeycomb reactor under surrounding ambient conditions, *J. Hazard. Mater.* 415 (2021) 125608.

APPENDIX A: LIST OF PUBLICATIONS

First Author

1. **N. Matyakubov**, D.B. Nguyen, S. Saud, Y.S. Mok, Enhancing the Selective Catalytic Reduction of NO_x at Low Temperature by Pretreatment of Hydrocarbons in a Gliding Arc Plasma, *Ind. Eng. Chem. Res.* 10.1021/acs.iecr.2c00025 (2022).
2. **N. Matyakubov**, D.B. Nguyen, S. Saud, I. Heo, S.-J. Kim, Y.J. Kim, J.H. Lee, Y.S. Mok, Effective practical removal of acetaldehyde by a sandwich-type plasma-in-honeycomb reactor under surrounding ambient conditions, *J. Hazard. Mater.* 415 (2021) 125608. <https://doi.org/10.1016/j.jhazmat.2021.125608>

Co-Author

3. D.B. Nguyen, **N. Matyakubov**, S. Saud, I.J. Heo, S.-J. Kim, Y.J. Kim, J.H. Lee, Y.S. Mok, High-Throughput NO_x Removal by Two-Stage Plasma Honeycomb Monolith Catalyst, *Environ. Sci. Technol.* 55 (2021) 6386-6396. <https://doi.org/10.1021/acs.est.1c00750>
4. D.B. Nguyen, S. Saud, **N. Matyakubov**, Y.S. Mok, S. Ryu, H. Jeon, S.B. Kim, Propagation of humidified air plasma in a sandwich-type honeycomb plasma reactor and its dependence on the ambient temperature and reactor diameter, *Plasma Sources Sci. Technol.* 29 (2020) 125016.
5. S. Saud, D.B. Nguyen, R.M. Bhattarai, **N. Matyakubov**, I. Heo, S.-J. Kim, Y.J. Kim, J.H. Lee, Y.S. Mok, Dependence of humidified air plasma discharge performance in commercial honeycomb monoliths on the configuration and key parameters of the reactor, *J. Hazard. Mater.* 404 (2021) 124024.

6. S. Saud, D.B. Nguyen, R.M. Bhattarai, **N. Matyakubov**, V.T. Nguyen, Y.S. Mok, Plasma-catalytic Ethylene Removal by a ZSM-5 Washcoat Honeycomb Monolith Impregnated With Palladium, *J. Hazard. Mater.* (2021) 127843.
7. S. Saud, D.B. Nguyen, S.-G. Kim, **N. Matyakubov**, V.T. Nguyen, Y.S. Mok, Influence of Background Gas for Plasma-Assisted Catalytic Removal of Ethylene in a Modified Dielectric Barrier Discharge-Reactor, *ACS Agricultural Science & Technology* (2021).
8. S. Saud, D.B. Nguyen, R.M. Bhattarai, **N. Matyakubov**, V.T. Nguyen, S. Ryu, H. Jeon, S.B. Kim, Y.S. Mok, Plasma-catalytic ethylene removal by a ZSM-5 washcoat honeycomb monolith impregnated with palladium, *J. Hazard. Mater.* 426 (2022) 127843.

APPENDIX B: LIST OF CONFERENCES

Nosir Matyakubov, Duc Ba Nguyen, Shirjana Saud, Iljeong Heo, Young Sun Mok ,
“Removal of acetaldehyde in a sandwich-type plasma-in-honeycomb reactor under humid condition” at the 60th anniversary of the 2020 Korea Society of Combustion Online Conference-
Sep 2020

Nosir Matyakubov, Duc Ba Nguyen, Shirjana Saud and Young Sun Mok,
“Application of non-thermal plasma-catalyst system for removal of VOC such as acetaldehyde at normal ambient pressure and temperature” at the KICHe-2021, Busan.

Nosir Matyakubov, Duc Ba Nguyen, Shirjana Saud, and Young Sun Mok,
“Removal of NO_x with n-heptane as a reductant via Non-Thermal Plasma Discharge in Honeycomb and Catalyst Stages” at the 63th KSIEC Meeting, November 2021 EXCO, Daegu.

Nosir Matyakubov, Duc Ba Nguyen, Shirjana Saud, and Young Sun Mok
“Acetaldehyde Removal by Air Plasma Discharge In a Honeycomb Plasma Reactor at Atmospheric Pressure and Room Temperature” at The Korean Society of Clean Technology Fall general meeting and academic conference-2021, Yeosu.